Available online at www.sciencedirect.com

ScienceDirect

Geochimica et Cosmochimica Acta 161 (2015) 219–247

Geochimica et Cosmochimica Acta

www.elsevier.com/locate/gca

Distinguishing and understanding thermogenic and biogenic sources of methane using multiply substituted isotopologues

D.A. Stolper [a,d,*], A.M. Martini [b], M. Clog [a], P.M. Douglas [a], S.S. Shusta [c], D.L. Valentine [c], A.L. Sessions [a], J.M. Eiler [a]

[a] Division of Geological and Planetary Sciences, 1200 E. California Blvd, Pasadena, CA, 91125, USA
[b] Department of Geology, Amherst College, Amherst, MA, USA
[c] Department of Earth Science and Marine Science Institute, University of California, Santa Barbara, CA, USA
[d] Current Address: Department of Geosciences, Princeton University, Princeton, NJ, USA

Received 19 December 2014; accepted in revised form 8 April 2015; available online 17 April 2015

Abstract

Sources of methane to sedimentary environments are commonly identified and quantified using the stable isotopic compositions of methane. The methane "clumped-isotope geothermometer", based on the measurement of multiply substituted methane isotopologues ($^{13}CH_3D$ and $^{12}CH_2D_2$), shows promise in adding new constraints to the sources and formational environments of both biogenic and thermogenic methane. However, questions remain about how this geothermometer behaves in systems with mixtures of biogenic and thermogenic gases and different biogenic environments. We have applied the methane clumped-isotope thermometer to a mixed biogenic–thermogenic system (Antrim Shale, USA) and to biogenic gas from gas seeps (Santa Barbara and Santa Monica Basin, USA), a pond on the Caltech campus, and methanogens grown in pure culture. We demonstrate that clumped-isotope based temperatures add new quantitative constraints to the relative amounts of biogenic vs. thermogenic gases in the Antrim Shale indicating a larger proportion (~50%) of thermogenic gas in the system than previously thought. Additionally, we find that the clumped-isotope temperature of biogenic methane appears related to the environmental settings in which the gas forms. In systems where methane generation rates appear to be slow (e.g., the Antrim Shale and gas seeps), microbial methane forms in or near both internal isotopic equilibrium and hydrogen-isotope equilibrium with environmental waters. In systems where methane forms rapidly, microbial methane is neither in internal isotopic equilibrium nor hydrogen-isotope equilibrium with environmental waters. A quantitative model of microbial methanogenesis that incorporates isotopes is proposed to explain these results.

1. INTRODUCTION

Understanding and quantifying the sources of methane in sedimentary environments is critical for studies of climate change, biogeochemical cycling, and energy exploration. The two dominant processes that generate methane in nature are (Wuebbles and Hayhoe, 2002): (i) methane generated by methanogenic archaea, known as 'biogenic' methane; and (ii) methane generated during the thermally-activated breakdown of larger organic molecules, termed 'thermogenic' methane. Identifying the relative contributions of these sources to a given accumulation of methane can be challenging because gases tend to migrate and mix in the subsurface (Tissot and Welte, 1978; England et al., 1987; Price and

* Corresponding author. Tel.: +1 626 395 3753.
E-mail address: dstolper@caltech.edu (D.A. Stolper).

http://dx.doi.org/10.1016/j.gca.2015.04.015
0016-7037/

Schoell, 1995; Hunt, 1996). However, this identification is the necessary first step in understanding the (bio)geochemistry of methane formation, gas flow, and ecology of microorganisms in the subsurface.

In many environments, thermogenic and biogenic gases can be distinguished using average or 'bulk' carbon- and hydrogen-isotope compositions combined with the relative abundances of methane to other hydrocarbon gases (e.g., Bernard et al., 1976; Schoell, 1980, 1983; Whiticar et al., 1986; Chung et al., 1988; Whiticar, 1999). These molecular and isotopic 'fingerprints' are a powerful and important starting point for establishing the origin of methane in nature, but they are not foolproof—some gases can appear both thermogenic and biogenic in these frameworks (Martini et al., 1996, 1998). Additionally, the end-member compositions of thermogenic and biogenic gases are sufficiently variable that it can be difficult to quantify their contributions to mixtures solely using isotopic and compositional parameters. Furthermore, the fundamental controls of the isotopic composition— especially the hydrogen isotopic composition—of biogenic and thermogenic methane remains poorly understood (Burke, 1993; Sugimoto and Wada, 1995; Whiticar, 1999; Valentine et al., 2004; Schimmelmann et al., 2006; Yoshioka et al., 2008; Ni et al., 2011; Hattori et al., 2012; Kawagucci et al., 2014). Key questions to consider when interpreting the meaning of the isotopic composition of biogenic methane are the importance of kinetic vs. equilibrium isotope effects during methanogenesis and, by extension, how reversible are the enzymatic processes involved in methane generation (Blair, 1998; Whiticar, 1999; Valentine et al., 2004; Penning et al., 2005).

1.1. New techniques to identify the source of methane in the environment

A potentially powerful way to distinguish biogenic from thermogenic methane is through the direct determination of a gas's formation temperature. For example, based on observations from environmental systems, biogenic gases in nature are generally thought to form below ~80 °C (Wilhelms et al., 2001; Valentine, 2011)—although laboratory methanogenic cultures can grow up to at least 122 °C (Takai et al., 2008). In contrast, based on both experiments and comparison to observations from sedimentary basins, thermogenic gases are thought to form above ~60 °C (Tissot and Welte, 1978; Quigley and Mackenzie, 1988; Hunt, 1996; Seewald et al., 1998; Seewald, 2003), and many models predict that most natural gases form at temperatures greater than ~150 °C (Quigley and Mackenzie, 1988; Seewald et al., 1998). Thus, knowledge of the formation temperature of a sample of methane could provide a fingerprint for its original formational environment and by extension, its source. Formation temperatures may be particularly distinctive and useful when combined with the established molecular and isotopic fingerprints discussed above as well as with existing geological and geochemical constraints.

New geothermometers based on the measurement of multiply substituted ('clumped') methane isotopologues (Ma et al., 2008; Tsuji et al., 2012; Stolper et al., 2014a,b; Ono et al., 2014a; Wang et al., in press) can constrain formation temperatures of methane. This is possible because the degree of clumped isotopic ordering, i.e., the clumped-isotope composition/distribution of a sample of methane (or any other molecule) that formed in isotopic equilibrium without further isotopic exchange after formation is a function of its formation temperature (e.g., Urey and Rittenberg, 1933; Wang et al., 2004; Eiler and Schauble, 2004; Schauble et al., 2006; Eiler, 2007, 2013; Ma et al., 2008; Yeung et al., 2012; Eiler et al., 2014a; Stolper et al., 2014a,b; Ono et al., 2014a; Webb and Miller, 2014). The potential to use clumped isotopes to measure methane formation temperatures has been demonstrated theoretically in several studies (Ma et al., 2008; Cao and Liu, 2012; Stolper et al., 2014a; Ono et al., 2014a; Webb and Miller, 2014).

The first demonstration that clumped-isotope distributions of methane could be measured at the sub-per-mil precisions necessary for geothermometry along with an experimentally generated temperature calibration was by Stolper et al. (2014a) using mass spectrometry. Stolper et al. (2014a) also provided evidence that thermogenic methane can yield clumped-isotope temperatures related to its formation temperatures. Following this, Stolper et al. (2014b) showed that clumped-isotope temperatures of biogenic and thermogenic methane from sedimentary basins are consistent with expected gas formation temperatures. Additionally, Stolper et al. (2014b) discussed (and showed in the Supplementary Materials) that biogenic methane can form without achieving an equilibrium distribution of clumped-isotopes, i.e., out of clumped-isotope equilibrium. They hypothesized that biogenic methane that resulted in reasonable clumped-isotope temperatures (and thus, by inference, formation in clumped isotopic equilibrium) resulted from the partial reversibility of enzymes involved in methanogenesis. Using an independent infrared spectroscopic method for measuring methane clumped-isotope distributions, Ono et al. (2014a) confirmed the results of the mass spectrometric measurements of Stolper et al. (2014a,b) that thermogenic methane yields clumped-isotope temperatures consistent with their formational environments. This demonstration that two different analytical techniques yield similar quantitative determinations of clumped-isotope distributions and inferred temperatures is an important demonstration of the validity of the application of clumped-isotope thermometry to natural systems.

Although clumped-isotope distributions of methane appear to reflect equilibrium distributions imprinted at the time of formation in many settings, including for some microbially sourced gases, in addition to the results of Stolper et al. (2014b) discussed above, Stolper et al. (2014c), Gruen et al. (2014), and Ono et al. (2014b) all presented preliminary results indicating that biogenic methane forms out of clumped-isotope equilibrium such that the clumped-isotope temperatures yield apparent temperatures that are too high to be formation temperatures. Stolper et al. (2014c) suggested that this disequilibrium reflects the methane's formation environment. Specifically, disequilibrium was suggested to occur in environments where methane generation rates are high, such as in organic-carbon-rich

environments (like a pond). Conversely, in subsurface environments such as sedimentary basins, where methane generation rates are slower, methane was suggested to form in clumped isotopic equilibrium. Stolper et al. (2014c) also showed that the clumped isotopic composition of biogenic methane was linked to the difference in D/H ratios of methane vs. the water it formed in: Specifically, when methane was found to be in clumped isotopic equilibrium and yielded reasonable clumped-isotope temperatures, it was also in D/H equilibrium with its formational waters. However, when the methane appeared to be out of clumped isotopic equilibrium, it was out of D/H isotopic equilibrium with its source waters. Following this, Eiler et al. (2014b) presented a quantitative model of microbial methanogenesis based on the hypothesis of Stolper et al. (2014b) that the degree of enzymatic reversibility during methanogenesis controls the clumped isotopic composition of methane. This model successfully linked the clumped isotopic composition of methane and the isotopic difference between methane, water and CO_2 to the overall reversibility of enzymes involved in methanogenesis. This preliminary work is developed and presented more fully here. Alternative hypotheses are that the generation of biogenic methane out of clumped isotopic equilibrium arises from kinetic isotope effects created via tunneling of hydrogen and deuterium atoms and/or other forms of kinetic isotope effect during hydrogenation reactions or reflect inheritance from substrates (Gruen et al., 2014; Ono et al., 2014b). In more recent work this same group (Wang et al., in press), confirmed that biogenic gases in some systems yield apparent methane clumped-isotope-based temperatures that are sensible, but that other biogenic systems yield apparent temperatures that represent methane formation of out of isotopic equilibrium. They additionally confirmed the correlation of D/H ratios of methane water vs. methane clumped-isotope compositions first presented by Stolper et al. (2014c) and developed a quantitative model similar to that shown by Eiler et al. (2014b) that also relates the generation of biogenic methane to enzymatic reversibility.

1.2. This study

Although initial results demonstrate promise in identifying the environment where methane forms, including distinguishing biogenic from thermogenic methane, clumped-isotope techniques have so far only been applied to methane from a small number of natural environments, most of which were dominantly either biogenic or thermogenic in origin (Stolper et al., 2014b; Wang et al., in press). Thus, it remains unclear whether these temperature constraints can yield quantitative insights into systems that contain a mixture of thermogenic and biogenic gases. Such mixtures could be difficult to untangle due to non-linear and unintuitive 'mixing effects' on the clumped isotope systematics of many gases [discussed below and more broadly in Eiler and Schauble (2004) and Eiler (2013)]. Additionally, distinguishing biogenic methane that forms out of isotopic equilibrium from thermogenic methane might be challenging (Gruen et al., 2014; Eiler et al., 2014b; Stolper et al., 2014b,c; Wang et al., in press).

To explore these issues, we have measured abundances of clumped isotopologues of methane in gases from the northern and western margin of the Antrim Shale in the Michigan Basin, which is known to contain a mixture of biogenic and thermogenic gases (Martini et al., 1996, 1998, 2003). We demonstrate that the measurements provide quantitative, novel insights into the origin of gases in the system. Specifically, the results indicate a higher abundance of thermogenic gases than previously inferred and add geologically grounded constraints on the source of the thermogenic component.

To place our results from the Antrim Shale system into a broader context, we also measured biogenic gases from laboratory cultures of methanogens and two other natural environments (gas seeps from the Santa Barbara and Santa Monica Basins and a pond from the Caltech campus). We demonstrate that the measured difference in the D/H ratio of biogenic methane versus that of the water in which the methane forms is correlated to the clumped-isotope composition. Using this relationship, we demonstrate that when methane is in clumped isotopic equilibrium, it is in heterogeneous equilibrium with water as well. We argue that this relationship is indicative of the importance of enzymatic reversibility in setting the isotopic composition of biogenic methane. The combined results from the Antrim Shale and these other settings indicate that the clumped isotopic composition of biogenic methane is sensitive to the environment in which the organisms grow. Specifically, as hypothesized by Stolper et al. (2014c), in systems where rates of microbial methanogenesis appear to be low, methane is formed in isotopic equilibrium with itself and other phases such as water. In contrast, rapid methane generation rates promote the formation of methane out of isotopic equilibrium with both itself and with other phases.

Based on these findings, following the initial work of Eiler et al. (2014b), we develop a quantitative model linking the physiology of methanogens to the measured clumped-isotope abundances of biogenic gases through the assumption that the enzymes involved in methanogenesis can operate reversibly. This model considers both kinetic- and equilibrium-based controls on the generation and isotopic composition of methane. We show that for fully reversible enzymatic conditions methane is generated in both internal isotopic (homogenous phase) and heterogeneous phase equilibrium with water and CO_2. In contrast, for partially irreversible enzymatic conditions, methane is formed out of both internal isotopic equilibrium and out of equilibrium with water and CO_2. This work highlights the key role clumped-isotope measurements can play in elucidating the thermodynamic conditions under which biogenic methane is generated.

2. GEOLOGICAL AND GEOCHEMICAL CONTEXT OF THE ANTRIM SHALE

The Antrim Shale subcrops below glacial drift deposits in the Michigan Basin (Fig. 1). It is Devonian in age, having formed during the Acadian orogeny as a distal facies of the Catskills delta complex (Gutschick and Sandberg, 1991).

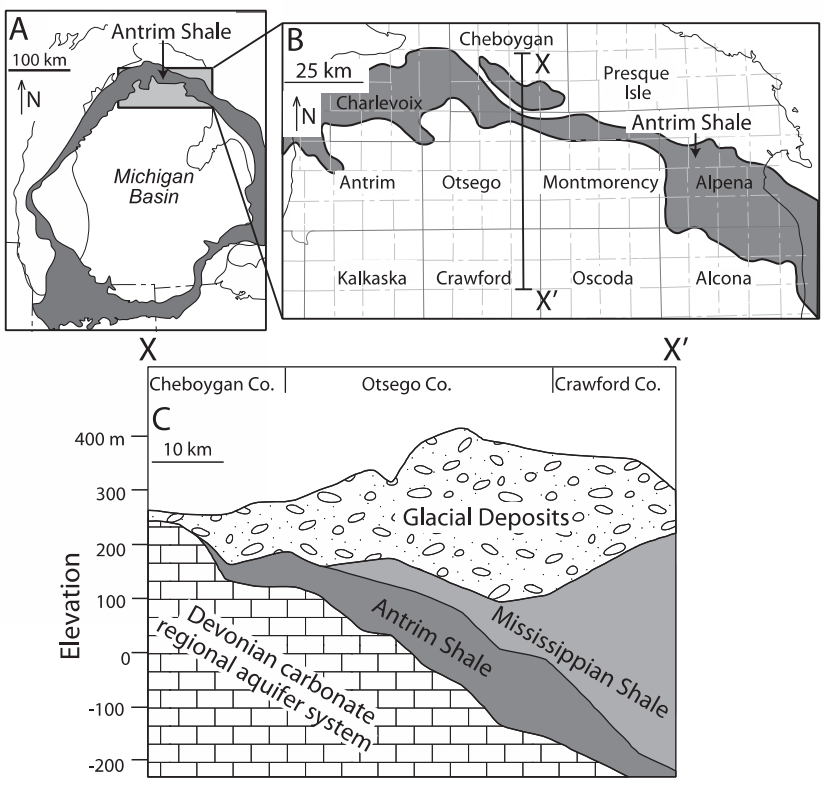

Fig. 1. Geological map and cross section of the Antrim Shale. Modified after Martini et al. (1998) and Martini et al. (2008). (A) Geological map of the Michigan Basin. In gray is the Antrim Shale. Note that it subcrops below glacial deposits. (B) Zoom in of A where the Antrim Shale subcrops in the northern margin. County names are given. (C) Cross section from X to X′ given in B.

The northern margin of the shale contains economically significant accumulations of natural gas (Martini et al., 1996, 1998) with over 12,000 wells drilled (Martini et al., 2008). It is considered to be an 'unconventional' shale-gas system in which the gases were formed and are stored *in situ*. There is evidence based on both isotopic and chemical constraints for extensive fluid migration within the northern margin of the Antrim Shale: specifically water from basinal brines is thought to have mixed in the northern margin with meteoric waters (Wilson and Long, 1993; Martini et al., 1998; McIntosh and Walter, 2005). This mixing is facilitated by fluid migration along extensive vertical fracture networks (Apotria and Kaiser, 1994; Martini et al., 1998) that are potentially important conduits for gas migration.

A key distinguishing feature of the northern margin Antrim Shale gases is that they are thought to be dominantly (>80%) microbial in origin with the remaining fraction (<20%) thermogenic (Martini et al., 1996, 1998). In fact, the Antrim Shale has been used as a model for microbially generated, unconventional shale-gas systems (Curtis, 2002). In addition to their economic importance, these systems have been proposed to play a role in regulating climate between glacial/interglacial cycles via storage and release of methane to the atmosphere (Formolo et al., 2008). There are three key pieces of evidence for the biological character of the northern margin gases: (i) Methanogens are present in formation waters (Waldron et al., 2007; Formolo et al., 2008; Kirk et al., 2012; Wuchter et al., 2013); (ii) δD values[1] of methane and water extracted (co-produced) with the methane are linearly correlated. Following Schoell (1980), this correlation was interpreted to indicate a biological origin for most (>80%) of the gas (Martini et al., 1996, 1998); and (iii) $\delta^{13}C$ values of co-produced CO_2 methane are high (>20‰; Martini et al., 1996, 1998, 2003), indicative of active hydrogenotrophic ($CO_2 + H_2$) methanogenesis in a closed system (e.g., Claypool and Kaplan, 1974). It is important to note that only the biogenic methane is hypothesized to have formed within the shales. The original formational site of the thermogenic component of the gases is poorly constrained. Proposed sources of the thermogenic gases include the northern margin itself (i.e., that it is self-sourced) or migration of gases into the northern margin along the fracture networks discussed above from more deeply buried expressions of the Antrim Shale in the mid-basin or older source rocks in the Michigan Basin (Martini et al., 1996, 1998, 2003). Consequently, the Antrim Shale provides a type example for studying both the mixing of thermogenic and biogenic gases in a relatively

[1] $\delta = (R/R_{std} - 1) \times 1000$ where $^{13}R = [^{13}C]/[^{12}C]$, $^{D}R = [D]/[H]$, $^{18}R = [^{18}O]/[^{16}O]$, and 'std' denotes the standard to which all measurements are referenced. For this paper all carbon measurements are referenced to VPDB and all hydrogen and oxygen measurements to VSMOW.

simple system and the behavior of methanogenic archaea in the 'deep biosphere' (Edwards et al., 2012).

Measurements of clumped isotopes provide an independent method to quantify the ratio of thermogenic and biogenic gases in the northern margin and thus test the proposal that the gases are dominantly microbial in origin. Specifically, if northern and western margin gases are dominantly biogenic and formed in internal isotopic equilibrium, the clumped-isotope temperatures should reflect current ambient temperatures in the shale (~10–30 °C; Martini et al., 1998).

3. METHODS

3.1. General methods and sample collection

We studied methane samples from a variety of economic wells from the northern margin of the Antrim Shale, and one sample from the western margin (Table 1). For each sample, we measured the δD and $\delta^{13}C$ values of methane ($\delta^{13}C_{CH4}$ and δD_{CH4}), relative abundances of C_1–C_4 alkanes, δD and $\delta^{18}O$ values of co-produced waters ($\delta D_{H2O,liquid}$ and $\delta^{18}O_{H2O,liquid}$), and $\delta^{13}C$ values of CO_2 ($\delta^{13}C_{CO2}$) in the gas phase. Clumped-isotope compositions of methane were also measured, and are reported as the combined signal of the mass-18 isotopologues ($^{13}CH_3D$ [~98%] and $^{12}CH_2D_2$ [~2%]). We also measured $\delta^{13}C$ values of ethane ($\delta^{13}C_{C2H6}$) for some samples.

Antrim Shale gases were sampled in duplicate directly from wellheads in stainless steel containers. One set was sent to Isotech Labs (Champaign, IL) and the other set sent to the Caltech. At Isotech, $\delta^{13}C$ values of CO_2 were measured using dual-inlet mass spectrometry with an external precision of ~0.1‰. Gas compositions (C_1/C_{2-4} ratios) were also measured at Isotech laboratories via gas chromatography using a Shimadzu 2014 and 2010 gas chromatographs equipped with flame ionization and thermal conductivity detectors. Relative precision was typically ±5% for C_{1-3} hydrocarbons and ±10% for larger hydrocarbons. $\delta D_{H2O,liquid}$ and $\delta^{18}O_{H2O,liquid}$ of co-produced waters were measured at Smith College using a Picarro L1102-i cavity ring-down spectroscopy analyzer. Precision was 0.2 ‰ for $\delta^{18}O_{H2O,liquid}$ and 0.5 ‰ for $\delta D_{H2O,liquid}$.

Table 1
Antrim Shale sample locations

Sample	County	Latitude	Longitude
Butcher C3-24	Ostego	45.059931	84.375012
Lake Horicon D4-15	Ostego	45.024263	84.692872
Marlatt 1-7	Montmorency	45.008181	84.251409
North Charlton A1-18	Ostego	45.083014	84.488447
State Charlton C4-18	Ostego	44.906223	84.476438
State Charlton C4-31	Ostego	45.059913	84.374974
State Loud B4-28	Montmorency	44.878911	84.073628
State Loud C2-31	Oscoda	44.860654	84.123699
State Charlton A3-32	Ostego	44.906019	84.476079
Weber A4-10[a]	Grand Traverse	44.741218	85.641642

[a] From the western margin. All others from the northern margin.

For Santa Barbara and Santa Monica Basin samples, gases were collected at the sea floor using an inverted funnel equipped with a stainless steel cylinder using the *ROV Jason* during cruise AT26-06 of the *R/V Atlantis*. Seeping gases were trapped using the inverted funnel and sealed in the cylinder for transport to the *R/V Atlantis* where they were subsampled for subsequent analyses. One subsample was used to measure gas composition at the University of California, Santa Barbara using the method described by Duffy et al. (2007). Another subsample was shipped to Caltech for analysis of clumped isotopes.

One sample of methane was extracted from a pond on Caltech's campus. A vacuum-evacuated 1 L Pyrex flask was connected to a vessel for collecting gas from sedimentary systems. Gases were released from the pond sediments manually through agitation and collected in the headspace of the initial vessel. Atmospheric gases were eliminated by first filling the vessel with pond water. The evacuated flask was then connected to the vessel via a rubber tube and opened, filling with pond-derived gas.

3.2. Description of clumped-isotope and ethane analyses and external reproducibility

Prior to isotopic analyses, methane and ethane were purified on a glass vacuum line as described in Stolper et al. (2014a), Stolper et al. (2014b), and Clog et al. (2014). $\delta^{13}C$, δD, and clumped-isotope compositions of methane and $\delta^{13}C$ of ethane were measured via mass spectrometry on a prototype, high-resolution isotope-ratio mass spectrometer, the MAT 253 Ultra (Eiler et al., 2013), at Caltech as described in Stolper et al. (2014a) and Stolper et al. (2014b) for methane and Clog et al. (2014) for ethane. External precisions for δD_{CH4} measurements were typically 0.13‰, 0.06‰ for $\delta^{13}C_{CH4}$ measurements and 0.03‰ for $\delta^{13}C_{C2H6}$ measurements.

Clumped-isotope compositions are expressed using Δ_{18} notation (Stolper et al., 2014a) where

$$\Delta_{18} = (^{18}R/^{18}R^{*} - 1) \times 1000, \quad (1)$$

and

$$^{18}R = ([^{13}CH_3D] + [^{12}CH_2D_2])/[^{12}CH_4]. \quad (2)$$

The brackets denote the molar concentration of the isotopologue as a fraction of all molecules of the compound of interest. R^{*} is the ratio expected for a random distribution of isotopes amongst all isotopologues (Stolper et al., 2014a). Δ_{18} values are reported in a reference frame in which 0‰ represents a random isotopic distribution. All samples are compared to (i.e., referenced against) a laboratory standard with a Δ_{18} value in this reference frame of 2.981‰, which was previously calibrated in the study of Stolper et al. (2014a). Δ_{18} values are converted into temperature (in Kelvin) via the equation (Stolper et al., 2014a):

$$\Delta_{18} = -0.0117\left(\frac{10^6}{T^2}\right)^2 + 0.708\left(\frac{10^6}{T^2}\right) - 0.337. \quad (3)$$

Samples were measured over 8 analytical sessions spanning 10 months including some overlap with measurement sessions for data reported in Stolper et al. (2014b).

External precision of measurements was monitored three ways. First, a standard differing in δD (+56‰), $\delta^{13}C$ (+33‰), and δ^{18} (+92‰[2]) as compared to the laboratory internal standard was measured multiple times in each analytical session. External precision for the Δ_{18} value across all measurements is ±0.23‰ (1 standard deviation, σ; $n = 19$), and differs in Δ_{18} by <0.04‰ from the long-term average of the standard over 2.5 years of measurements (being slightly too positive). Second, gases equilibrated on nickel catalysts at 500 °C were measured in all sessions (Stolper et al., 2014a). External precision across the sessions is ±0.28‰ (1σ; $n = 17$) and differs by <0.06‰ in Δ_{18} from the long-term (2.5 year) average (again being slightly too positive). Additionally, no statistically significant dependence of Δ_{18} values on the bulk isotopic composition of the heated gases (monitored using a 300‰ range in δ^{18} values) was observed (Fig. A1). Third, 8 Antrim Shale gases and 1 Santa Monica Basin gas were measured multiple times in different sessions. Additionally, the Antrim Shale samples were purified by different users and contain significant quantities of gases other than methane. Thus, replicate analysis of these samples should provide constraints on the overall reproducibility of the Δ_{18} measurements that incorporates both sample preparation and mass-spectrometric measurements. The external precision for Δ_{18} for the samples is ±0.24‰ (1σ, $n = 20$). One Antrim sample (North Charlton A1-18), measured 3 times, yielded a single outlier Δ_{18} value compared to the others and this value is excluded from all further discussion. Exclusion of this outlier yields an external precision for Δ_{18} measurements of 0.17‰ (1σ, $n = 19$).

We thus conclude that Δ_{18} external precisions are ~0.25‰, consistent with internal, counting-statistics-derived errors for a single measurement of 0.24 to 0.27‰ (Stolper et al., 2014a). In two sessions, drift in the standard used to normalize data from a measurement session to a unified δD and Δ_{18} reference frame (as described in Stolper et al., 2014a) was observed. We corrected for this drift by measuring the standard used for the correction multiple times over the course of these sessions and assumed the values required for the correction for a sample measured on a different day changed linearly with time between observations of the standard. The quality of the correction was checked through multiple measurements of a secondary standard (the one described above which differs in δD, $\delta^{13}C$ and δ^{18} as compared to the laboratory reference standard) in all sessions and re-analysis of at least some samples in other sessions. For both sessions, final average Δ_{18} values of the secondary standard were within 1 standard error (s.e.) of its long-term average (longer term average $\Delta_{18} = 1.71$): 1.79 ± 0.07 (1 s.e., $n = 2$) and 1.56 ± 0.15 (1 s.e., $n = 4$). Additionally, the overall external precision of the Antrim Shale samples, including those observed in these sessions, does not differ from the external precision of other measured standards and 500 °C heated gases.

[2] $\delta^{18} = ({}^{18}R_{sample}/{}^{18}R_{standard} - 1) \times 1000$ where ${}^{18}R = ([{}^{13}CH_3D] + [{}^{12}CH_2D_2])/[{}^{12}CH_4]$.

3.3. Methanogen pure-culture growth conditions and considerations

Pure cultures of *Methanothermobacter marburgensis* and *Methanosarcina barkeri* (species of methanogens) were grown at the University of California, Santa Barbara in an H_2/CO_2 atmosphere following Boone et al. (1989), at constant temperatures from 30 to 70 °C. Samples were shaken to ensure mixing of H_2 into the solution. Before sampling of methane, culture media was removed from the culture bottles. Methane was removed from the culture bottles with a gas-tight syringe (Vici), injected onto a vacuum glass line, and then purified as described in Stolper et al. (2014a,b). These samples are more depleted in δ^{18} relative to our working gas standard by ~200 to 400‰ and are outside of the normal range of bulk isotopic composition of samples usually measured. To ensure no measureable bias exists for measurements of gases with significantly more depleted δ^{18} values than the standards, two biogenic gases ($\delta^{18} = -180$ to -200‰) were heated in the presence of nickel catalysts to promote internal isotopic equilibrium at 500 °C following Stolper et al. (2014a). These gases yielded a Δ_{18} value of 1.03 ± 0.28 (1 s.e.), identical within error to the long term average for 500 °C heated gases, 1.06 ± 0.05 ($n = 21$, 1 s.e.). However we note that two samples measured were significantly more depleted in δ^{18} (by ~200‰) than the biogenic gases catalytically equilibrated at 500 °C (the 30 °C and 37 °C experiments). Thus there is the potential that an analytical artifact for these very low δ^{18} samples exists that was not tested for by our study of heated, low δ^{18} gases. Regardless, any inaccuracies up to ~ ± 2‰ for these samples, i.e., an order of magnitude larger than the stated 1σ error bars, would not affect any interpretation of these measurements.

$\delta D_{H2O,liquid}$ for one pure-culture experiment (65 °C *M. marburgensis* experiment) and the Caltech Pond samples were measured at Caltech using a spectroscopic Liquid-Water Isotope Analyzer (Los Gatos Research Inc.) as described in Feakins and Sessions (2010). Samples were standardized to the VSMOW/VSLAP scale by measuring standards of known isotopic composition that bracketed the δD values of the samples. Typical precision for $\delta D_{H2O,liquid}$ measurements for this instrument is ~<1‰ (Feakins and Sessions, 2010). $\delta D_{H2O,liquid}$ values were not measured for all culture media, which were prepared with the same water source but at different times. We assume that all media had the same δD value with a conservative 1σ error of 25‰ for the instances where the value was not measured.

3.4. Calculations of expected differences in δD_{H2O} vs. δD_{CH4}

We calculated the expected equilibrium isotopic difference between δD_{CH4} and $\delta D_{H2O,liquid}$, i.e., $\alpha_{CH4-H2O,liquid}$, where $\alpha_{A-B} = (R_A/R_B)$. To do this, we first calculated $\alpha_{CH4-H2O,vapor}$ (where 'H_2O, vapor' refers to water in the vapor phase) as a function of temperature using the theoretically derived data from Richet et al. (1977). The derived equations are given in Table 2. In Richet et al. (1977), two theoretical datasets are available to calculate

Table 2
Theoretically derived temperature dependencies for $\alpha_{CH4–H2O,vapor}$ and $\alpha_{CH4–CO2}$

Type[a]	Equation[a,b]
Harmonic	$1000\ln(\alpha_{CH4H2O,vapor}) = 0.8576(1000/T)^4 - 14.412(1000/T)^3 + 88.483(1000/T)^2 - 209.56(1000/T) + 60.553$
Anharmonic	$1000\ln(\alpha_{CH4H2O,vapor}) = 1.1014(1000/T)^5 - 11.537(1000/T)^4 + 38.890(1000/T)^3 - 20.448(1000/T)^2 - 129.250(1000/T) + 21.701$
Harmonic	$1000\ln(\alpha_{CH4CO2}) = 0.6196(1000/T)^3 - 6.628(1000/T)^2 - 6.025(1000/T) + 3.071$

[a] Equations derived from Richet et al. (1977).
[b] T is in Kelvin.

$\alpha_{CH4–H2O,vapor}$, one that incorporates anharmonicity in the reduced partition functions of methane and one that does not (i.e., is harmonic). These models disagree strongly at low temperatures, yielding, for example, a 70‰ difference in $\alpha_{CH4–H2O,vapor}$ at 20 °C. Perhaps surprisingly, there are no independent experimentally or environmentally derived constraints to indicate which is correct. In the face of these uncertainties, we simply used the average of the two model estimates at a given temperature to calculate $\alpha_{CH4–H2O,vapor}$. This estimate was then combined with the experimentally derived fractionation factor between liquid water and vapor from Horita and Wesolowski (1994), resulting in an estimated value for $\alpha_{CH4–H2O,liquid}$. We did not use the experimentally calibrated $\alpha_{CH4–H2}$ calibration provided by Horibe and Craig (1995) (in combination with other fractionation factors to arrive at $\alpha_{CH4–H2O,liquid}$) as it is only calibrated at temperatures greater than 200 °C. As our interest in using this calibration (see below) is for microbial environments, which range in temperature from ~0 to 120 °C (all samples examined here were generated below 70 °C), we consider it more accurate to use the theoretical forms given in Richet et al. (1977). We note though, that the calibration of $\alpha_{CH4–H2}$ from Horibe and Craig (1995) combined with the calibration for $\alpha_{H2–H2O,vapor}$ from Richet et al. (1977) and $\alpha_{H2O,liquid–H2O,vapor}$ from Horita and Wesolowski (1994) results in a calibration that falls between those derived using the harmonic and anharmonic calculations for $\alpha_{CH4–H2O,vapor}$ from Richet et al. (1977) with $\alpha_{H2O,liquid–H2O,vapor}$ from Horita and Wesolowski (1994) discussed above.

4. MIXED-SOURCE GASES OF THE ANTRIM SHALE

4.1. Stable-isotope systematics and chemical/physical measurements of the Antrim Shale

Measured isotopic and physical/chemical values for Antrim Shale gases are provided in Table 3 and Fig. 2. Samples measured in this study are similar in isotopic composition and $C_1/C_{2–4}$ ratios to those measured previously by others (Fig. 2a, c, and e; Martini et al., 1996, 1998, 2003). Gas-well temperatures range from 16 to 24 °C (Table 3).

The $\delta^{13}C_{CH4}$ values of all measured gases vary by less than 3‰, ranging from −50 to −53‰ (Fig. 2c and d). Historically, $\delta^{13}C_{CH4}$ values <−60‰ have often been considered indicative of biogenic gases, while those ~>−50‰ indicative of thermogenic gases (Schoell, 1980; Whiticar, 1999), though the actual ranges in nature may have a larger overlap (e.g., Tang et al., 2000; Valentine et al., 2004). Regardless, the $\delta^{13}C$ values observed in the Antrim Shale gases fall between these historic ranges and, as discussed by others, do not yield strong constraints on the origin of the methane (Martini et al., 1996, 1998; Whiticar, 1999). As observed in other northern margin gases, all $\delta^{13}C_{CO2}$ values are >20‰ (Table 3; Martini et al., 1996, 1998, 2003). Also, δD_{CH4} and $\delta D_{H2O,liquid}$ values are correlated, following a similar linear trend as observed previously (Fig. 2e). As discussed above, these two observations were previously used by Martini et al. (1996) to hypothesize that the northern margin gases are dominantly biogenic in origin. However, a proportion of thermogenic gases must be present in the samples because some contain significant quantities of $C_{2–4}$ alkanes with $C_1/C_{2–4}$ ratios as low as 8 (i.e., 11% $C_{2–4}$ alkanes relative to all $C_{1–4}$ alkanes; Table 3). This is because $C_{2–4}$ alkanes are thought to be of thermogenic origin in the Antrim Shale (Martini et al., 2003). Similarly low $C_1/C_{2–4}$ ratios ($C_1/C_{2–4} = 12$; Fig. 2a) occur in other northern margin gases (Martini et al., 1998). Finally, as observed in previous studies (Martini et al., 1996, 1998), the $C_1/C_{2–4}$ ratio is related to δD_{CH4} values, such that gases with more enriched δD_{CH4} values have lower $C_1/C_{2–4}$ ratios (Fig. 2a). This relationship is consistent with gases with more enriched δD_{CH4} values having a greater proportion of thermogenic gas.

4.2. Δ_{18}-based temperatures

Measured Δ_{18} temperatures average 67 °C, range from 40 to 115 °C (Table 3), and correlate with many of the other measured parameters. For example, a hyperbolic relationship exists between Δ_{18} temperatures and $C_1/C_{2–4}$ ratios, with hotter temperatures corresponding to lower $C_1/C_{2–4}$ values (Fig. 2b). Δ_{18} temperatures are also linearly correlated with $\delta D_{H2O,liquid}$ (Fig. 2f) and δD_{CH4} (Fig. 2g), with hotter temperatures corresponding to more enriched $\delta D_{H2O,liquid}$ and δD_{CH4} values. Despite the relatively small variation of $\delta^{13}C_{CH4}$ in Antrim shale gases (and a general lack of correlation with other geochemical properties), we note a weak linear relationship between $\delta^{13}C_{CH4}$ and Δ_{18} temperatures ($r^2 = 0.31$; Fig. 2d). This relationship or lack thereof is discussed in more detail below in the context of a quantitative mixing model (Section 4.2).

The relationships between Δ_{18} temperatures and various other isotopic and compositional parameters support the hypothesis that the northern margin gases are a mixture of lower temperature biogenic gases with higher

Table 3
Physical and isotopic measurements of Antrim Shale samples

Sample	Well T (°C)	δD_{CH4} (‰)[a]	±	$\delta^{13}C_{CH4}$ (‰)[b]	±	Δ_{18} (‰)	±	$T_{\Delta 18}$ (°C)[c]	±	$\delta D_{H2O,liquid}$ (‰)[a]	$\delta^{18}O_{H2O,liquid}$ (‰)[a]	$\delta^{13}C_{CO2}$ (‰)[b]	C_1/C_{2-4}	$\delta^{13}C_{C2H6}$ (‰)[b,d]	n
Butcher C3-24	20	−247.6	0.15	−50.3	0.04	5.60	0.20	43	6	−81.8	−12.2	25.5	10225	–	3
Lake Horicon D4–15	16	−240.4	0.01	−53.0	0.05	4.80	0.05	72	2	−76.1	−11.4	22.8	46	−45.6	2
Marlatt 1-7	23	−240.4	0.13	−50.9	0.05	5.30	0.28	53	10	−62.4	−10.5	26.9	782	−33.9[e]	2
North Charlton A1-18	16	−256.5	0.07	−53.2	0.03	5.68	0.13	40	4	−88.1	−13.4	24.1	873	−36.2[e]	3
State Charlton C4-18	16	−233.4	0.22	−52.2	0.02	4.65	0.00	78	0.1	−46.5	−7.3	22.5	27	−45.6	2
State Charlton C4-31	16	−247.4	0.14	−51.1	0.04	5.30	0.11	53	4	−77.7	−11.9	23.9	393	−34.8[e]	2
State Loud B4-28	24	−225.8	0.20	−52.8	0.03	4.09	0.19	104	9	−31.9	−5.1	23.1	9	−52.9	2
State Loud C2-31	19	−221.6	0.04	−53.2	0.01	3.87	0.01	115	0.4	−23.9	−3.9	22.3	8	−48.8	2
State Charlton A3-32	16	−211.3	0.11	−51.7	0.01	4.94	0.24	67	9	−22.5	−3.7	21.7	8	−45.4	1
Weber A4-10	16	−246.2	0.12	−51.9	0.01	5.60	0.27	43	9	−72.8	−11.1	24.7	153	–	1

[a] Referenced to VSMOW.
[b] Referenced to the VPDB scale.
[c] Δ_{18}-based temperature.
[d] Typical 1σ precision of ±0.03.
[e] From Kirk et al. (2012).

temperature thermogenic gases. For example, samples previously interpreted to be dominantly biogenic, those with more depleted δD_{CH4} values and higher C_1/C_{2-4} ratios (Martini et al., 1996, 1998, 2003) yield the lowest Δ_{18} temperatures while samples with lower C_1/C_{2-4} ratios yield the highest temperatures. The meaning of the Δ_{18} values of the samples, which, based on previous criteria, should contain significant quantities of biogenic methane is not straightforward. For example, the Δ_{18} temperatures of the thermogenic and biogenic end members could reflect the actual gas formation temperatures (Stolper et al., 2014b). Alternatively, the Δ_{18} temperatures of the biogenic end member could be influenced by kinetic isotope effects that have been observed in some microbial systems (Stolper et al., 2014b,c; Gruen et al., 2014; Ono et al., 2014b; Eiler et al., 2014b; Wang et al., in press). Thus, it is not clear whether we should interpret the low measured Δ_{18} temperatures of biogenic gases as an indication of their actual formation temperatures, or instead as some non-equilibrium isotopic signature. As will be discussed and developed in the following sections, multiple lines of evidence indicate that the Δ_{18}-based temperatures of the biogenic end-member gases are ~20 °C, the current temperature of the shales, and thus that the biogenic component of the gases was formed in clumped isotopic equilibrium.

4.3. Mixing model

The relationships between Δ_{18} temperature and δD_{CH4}, $\delta D_{H2O,liquid}$, and C_1/C_{2-4} values suggests that the Δ_{18} temperatures relate to the amount of thermogenic and biogenic gas in the system. In order to explore the feasibility of this quantitatively, a mixing model was created. This model assumes that there are two end members of gases mixed together, one a biogenic gas formed at lower temperatures and the other a thermogenic gas formed at higher temperatures. In order to create this model, end-member values for the Δ_{18} temperatures, δD_{CH4} and δD_{H2O} values, and C_1/C_{2-4} ratios had to be assigned. In choosing these end-member values, we incorporated as many external constraints as possible. Thus the model can serve as a test of the plausibility of the measured Δ_{18} temperatures. I.e., we can ask whether the mixing model is both self-consistent with one or more of the trends defined by the samples studied here and, more broadly, with the other measured properties of these and related gases.

Assumed compositions for the thermogenic and biogenic end-member components of our mixing model are given in Table 4. Of these, two compositional parameters ($\delta^{13}C_{CH4}$ and Δ_{18} of both end members) are discussed in detail here. $\delta^{13}C_{CH4}$ end-member values were chosen assuming, as observed by the weak linear relationship between $\delta^{13}C_{CH4}$ and Δ_{18}-temperature (Fig. 2d), that the biogenic end member has a more enriched $\delta^{13}C_{CH4}$ value than the thermogenic end member. Then, the highest measured $\delta^{13}C_{CH4}$ value of a northern margin gas with C_1/C_{2-4} ratios >500 was taken for the biogenic component and lowest $\delta^{13}C_{CH4}$ value of gases with $C_1/C_{2-4} < 100$ for the thermogenic component (Table 4). However, the potential range of $\delta^{13}C_{CH4}$ end-member values varies by 9‰,

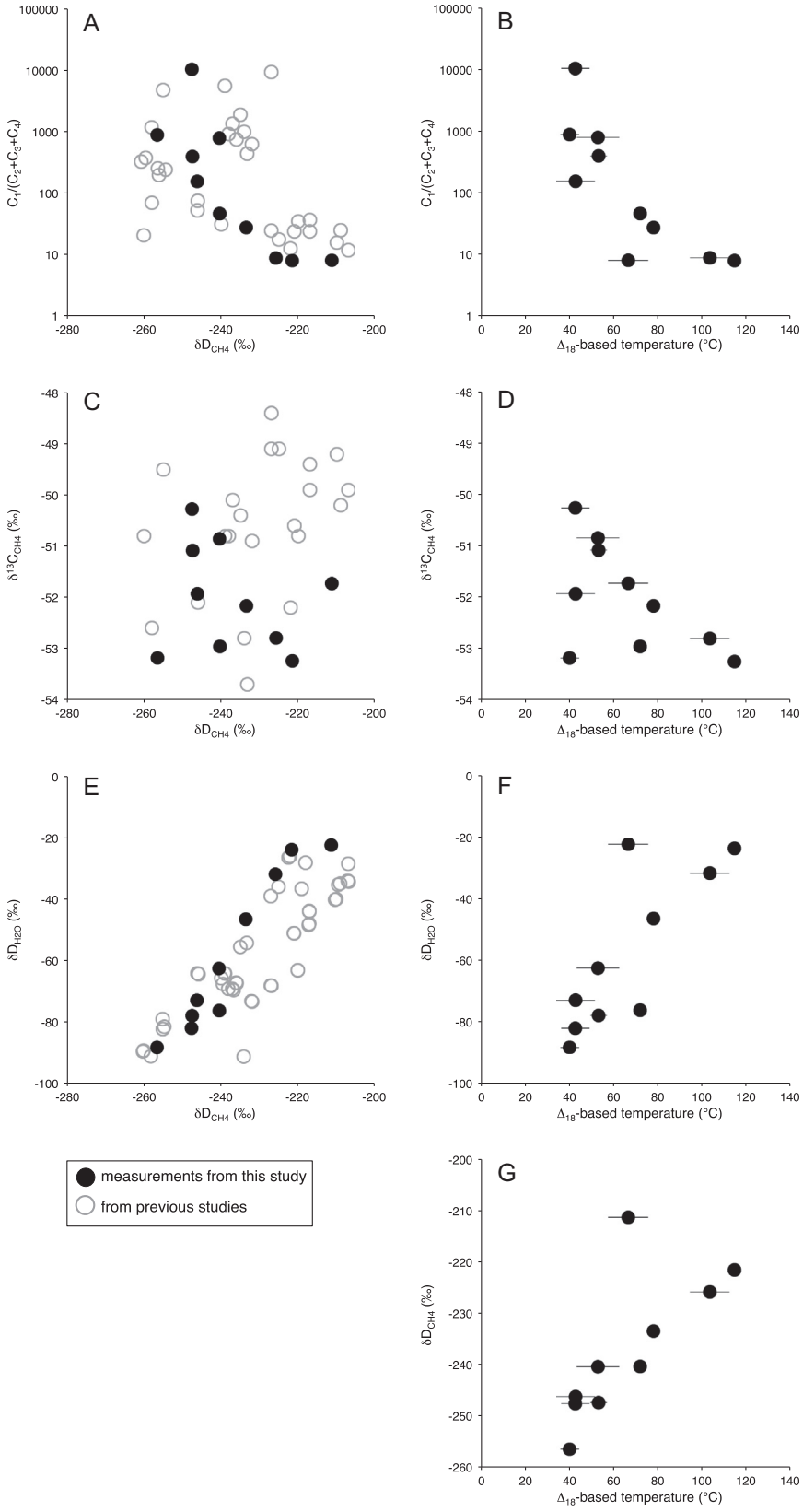

Fig. 2. Measured data from Antrim Shale samples. Error bars are all 1σ and are not displayed if they are smaller than the symbol. Data from previous studies come from Martini et al. (1996, 1998, 2003). Panels on the left plot properties vs. δD_{CH4}. Panels on the right plot properties vs. Δ_{18}-based temperatures. (A) C_1/C_{2-4} vs. δD_{CH4}. (B) C_1/C_{2-4} vs. Δ_{18}-based temperatures. (C) $\delta^{13}C$ vs. δD_{CH4}. (D) $\delta^{13}C$ vs. Δ_{18}-based temperatures. (E) $\delta D_{H2O,liquid}$ vs. δD_{CH4}. (F) $\delta D_{H2O,liquid}$ vs. Δ_{18}-based temperatures. (G) δD_{CH4} vs. Δ_{18}-based temperatures.

significantly larger than the range of samples measured here (3‰; Fig. A2). Thus, our choice of end-member $\delta^{13}C_{CH4}$ values can be thought of as plausible but non-unique. Importantly, the $\delta^{13}C_{CH4}$ variations among Antrim methane samples are sufficiently small and poorly correlated with other isotopic and molecular indices that this uncertainty has little bearing on other elements of our model: Any choice of $\delta^{13}C_{CH4}$ values from the possible range has no significant quantitative impact on the resultant model (Fig. A2). For these reasons we include $\delta^{13}C$ values in Table 4 in the interest of completeness but do not discuss them further.

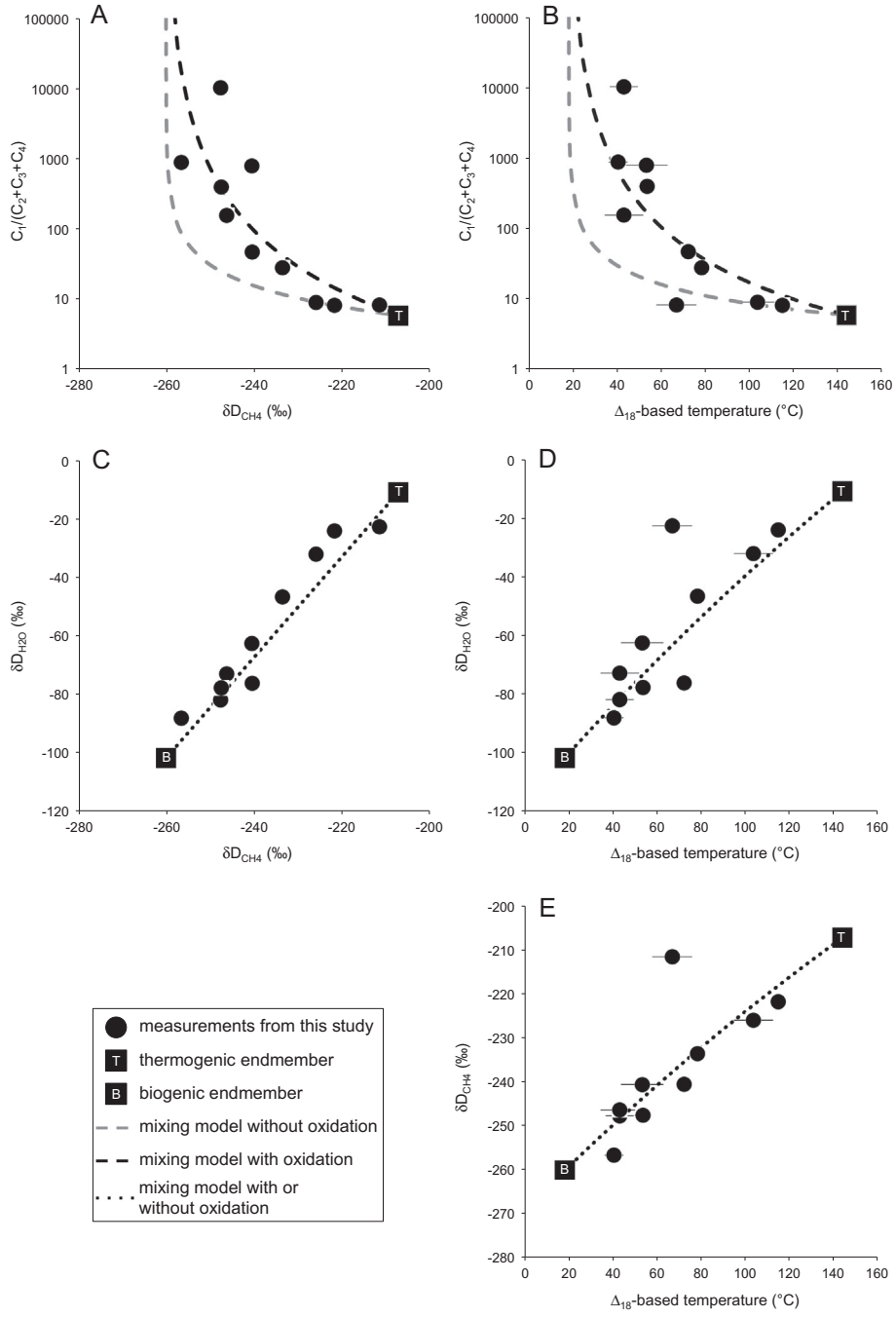

Fig. 3. Comparison of the end-member mixing models with or without oxidation of C_{2-4} hydrocarbons. Error bars are all 1σ and are not displayed if they are smaller than the symbol. For C, D, and E, both mixing models yields identical results as the oxidation of C_{2-4} hydrocarbons has no effect on the methane's or the formation water's isotopic composition. Panels on the left plot properties vs. δD_{CH4}. Panels on the right plot properties vs. Δ_{18}-based temperatures. (A) C_1/C_{2-4} vs. δD_{CH4}. (B) C_1/C_{2-4} vs. Δ_{18}-based temperatures. (C) $\delta D_{H2O,liquid}$ vs. δD_{CH4}. (D) $\delta D_{H2O,liquid}$ vs. Δ_{18}-based temperatures. For this mixing space, it is presumed that the mixing ratios of the gases are equivalent to the mixing ratios of the waters. (E) δD_{CH4} vs. Δ_{18}-based temperatures.

For this model, we have assumed that the biogenic Δ_{18} temperature reflects current temperatures in the Antrim Shale (~20 °C). We will validate this in a variety of ways in the following sections, but in first constructing this mixing model, we simply adopt it as an assumption. We do not know of any independent constraints on the maximum formation temperature of the thermogenic end member, because its source is not known (Martini et al., 1996, 1998). We estimated this temperature ($T_{\Delta 18}$) using the observed linear relationship between δD_{CH4} and Δ_{18} temperature (Fig. 2g; $T_{\Delta 18}$ (°C) = 2.33 × δD + 626) with independent constraints on the maximum δD_{CH4} of the thermogenic end member, −207‰ (from the northern margin; Martini et al., 1998). For this analysis, we excluded the one significant outlier point in Fig. 2g (State Charlton A3-32, δD = −211‰, $T_{\Delta 18}$ = 67 °C). Application of our regression then implies a maximum Δ_{18} temperature of 144 °C (±11 °C, 1σ). Although this temperature is higher than those estimated for maximum burial temperatures of the northern margin of the Antrim Shale (see below), it is consistent with previously measured peak temperatures (based on fluid inclusions) of ~150 °C (and perhaps as high as 175 °C) in the deeper-buried Devonian-aged, oil-producing Dundee Formation in the Michigan Basin (Luczaj et al., 2006) and previous suggestions that the thermogenic gases could have formed outside of the northern margin (Martini et al., 1996, 1998).

A key aspect of mixing of clumped isotopic compositions to consider is that Δ_{18}-based temperatures of a mixture are not linear functions of the Δ_{18}-based temperatures of the end members. This non-linearity occurs because: (i) Δ_{18} values have a non-linear dependence on temperature (Eq. (3) above)—thus, although Δ_{18} values can be linear mixtures of end members, Δ_{18}-based temperatures need not; and (ii), Δ_{18} values of mixtures depend not only on the Δ_{18} value of the end members, but the δD_{CH4} and $\delta^{13}C_{CH4}$ values as well (Stolper et al., 2014a,b). In the Antrim Shale, the $\delta^{13}C_{CH4}$ and δD_{CH4} values of the biogenic and thermogenic end members do not differ enough for this second non-linearity to matter: for example, the differences in Δ_{18} values of the mixtures using the approximation that Δ_{18} values mix linearly vs. doing the calculation precisely are less than 0.1‰. This is less than half the analytical precision of a single measurement and thus unimportant for all conclusions made here—for the calculations here, all mixing is done exactly and all non-linearities included.

Modeled isotopic compositions for mixtures of these two end-member gases are shown in Fig. 3. The model agrees well with measured data for δD_{CH4} vs. δD_{H2O} (Fig. 3c), Δ_{18} temperatures vs. δD_{H2O} (Fig. 3d), and δD_{CH4} vs. Δ_{18} temperature (Fig. 3e). Poorer matches between the mixing model and the measured data occur for C_1/C_{2-4} vs. δD_{CH4} (Fig. 3a) and vs. Δ_{18} temperature (Fig. 3b). The poor match of C_1/C_{2-4} ratios vs. the isotopic values was expected because the abundances of ethane, propane, and butane are not thought to be controlled solely by mixing of end members in the Antrim Shale, but instead by a combination of mixing and microbial oxidation (Martini et al., 2003). The oxidation of ethane and propane is supported by the correlation of $\delta^{13}C_{C2H6}$ values with the concentration of ethane such that as ethane concentrations decrease (C_1/C_{2-4} rises), $\delta^{13}C_{C2H6}$ values increase (Fig. 4; Martini et al., 2003). A significant change in the $\delta^{13}C$ value

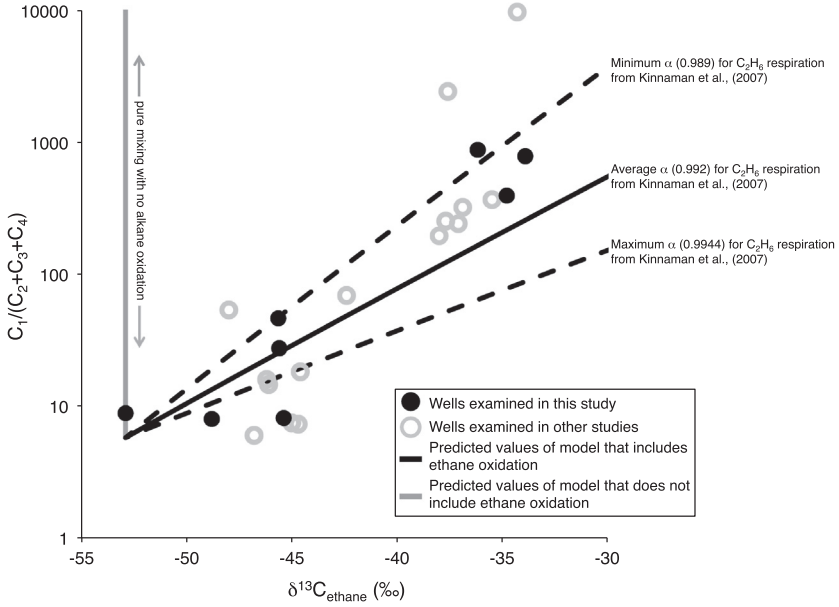

Fig. 4. Mixing model's prediction of the $\delta^{13}C$ of ethane as a function of the C_1/C_{2-4} ratio. $\delta^{13}C$ values of ethane are from this study and from previous measurements from Martini et al. (2003) and Kirk et al. (2012). Fractionation factors (α) for ethane oxidation are equal to $(1000 + \delta^{13}C_{C2H6,respired})/(1000 + \delta^{13}C_{C2H6,residual})$, where 'respired' refers to the ethane that is respired by microbes and 'residual' refers to the remaining ethane. α values for ethane oxidation are all from Kinnaman et al. (2007). The thermogenic end member is assumed to have a $\delta^{13}C$ value of −52.9 ‰ and C_1/C_{2-4} of 5.8. See text for details.

of ethane cannot occur solely due to mixing when one end member contains no or very little ethane. Oxidative consumption of ethane, on the other hand, will cause $\delta^{13}C_{C2H6}$ values to increase (Kinnaman et al., 2007; Kniemeyer et al., 2007; Valentine et al., 2010).

We incorporated this microbial hydrocarbon oxidation into the mixing model by assuming that its extent is correlated with the amount of biogenic gas in the mixture. We have modeled this by assuming that the amount of microbial oxidation is equal to the mixing ratio of biogenic gas raised to a power (with maximum and minimum mixing ratios of 0 and 1 respectively). We found the power, 2.1, that best fit the data by minimizing the combined residuals of the modeled and measured $\log(C_1/C_{2-4})$ values as a function of δD_{CH4} and Δ_{18} temperature (Fig. 3a and b). Importantly, both the C_1/C_{2-4} vs. δD_{CH4} and vs. Δ_{18} temperature can be fit with the same amount of oxidation as a function of the biogenic mixing ratio. Although this is an arbitrary parameterization of microbial oxidation, the essential point is that the data are consistent with increasing C_{2+} oxidation at the same time more microbial gas is added. Importantly, both the C_1/C_{2-4} vs. δD_{CH4} and vs. Δ_{18} temperature relationships can be fit with the same parameterization.

In contrast to ethane and propane, we have assumed that methane oxidation is not significant in the northern margin following Martini et al. (2003). This is based on the relatively small range of $\delta^{13}C_{CH4}$ values (<3‰) and on the absence of covariation between δD_{CH4} and $\delta^{13}C_{CH4}$ (Fig. 2c). Significant amounts of methane oxidation generally result in measurable increases in both the $\delta^{13}C$ and δD values of the residual methane (Whiticar, 1999). Additionally, C_{2-4} alkanes are often oxidized orders of magnitude more rapidly than methane in natural systems (Valentine et al., 2010). However, we note that recent laboratory manipulations suggest that anaerobic microbial oxidation of methane may be occurring within the Antrim Shale (Wuchter et al., 2013). Regardless, the effect of microbial oxidation on Δ_{18} values of residual methane is unknown and thus currently difficult to incorporate into our model.

4.4. A test of the mixing model

Importantly, the model can be tested using an entirely independent constraint, the $\delta^{13}C$ of ethane. Specifically, the model calculates the amount of ethane oxidation occurring as a function of the mixing ratio of biogenic relative to thermogenic gases (or C_1/C_{2-4} ratios). Therefore, if the carbon isotopic fractionation associated with microbial ethane oxidation is known, the model explicitly predicts the $\delta^{13}C_{C2H6}$ of the residual ethane. We performed this test using a Rayleigh distillation model (Criss, 1999) with a range of independently measured carbon-isotope fractionation factors for microbial ethane oxidation from Kinnaman et al. (2007), an initial C_1/C_{2-4} ratio of 5.8 for the thermogenic end member (as in the model above), and initial $\delta^{13}C_{C2H6}$ value of −52.9, the lowest observed $\delta^{13}C_{C2H6}$ from the northern margin gases. We note that the fractionation factors used here are for aerobic ethane oxidation as these are the only known isotopic fractionation factors for microbial ethane oxidation.

The model's predicted $\delta^{13}C_{C2H6}$ vs. C_1/C_{2-4} values are consistent with the measured values from wells sampled in this study and other measured wells (Fig. 4). Although some measurements fall outside of the predicted envelope of values (Fig. 4), these divergences are not surprising as it is unlikely that all samples start with the exact same C_1/C_{2-4} ratio or ethane $\delta^{13}C$ value. Regardless, the agreement between the modeled vs. measured $\delta^{13}C_{C2H6}$ values further demonstrates the plausibility of the mixing/oxidation model we present and provides an independent check on the calculated amount of oxidation occurring in the samples. The model also helps to validate our assumption that methanogens in the Antrim Shale generate methane with a Δ_{18}-based temperature near ~20 °C. If that temperature was 40 to 45 °C, with no microbial oxidation of C_{2-4} gases, then the measured $T_{\Delta 18}$ vs. C_1/C_{2-4} data could be reproduced by the model, but the δD_{CH4} vs. C_1/C_{2-4} would still result in a misfit. Adding microbial oxidation to the model would correct the fit for C_1/C_{2-4} vs. δD_{CH4}, but would then result in a misfit for $T_{\Delta 18}$ vs. C_1/C_{2-4}. In other words, only model parameters with biogenic methane at or near internal isotopic equilibrium at ~20 °C can satisfy all of the measured isotopic and compositional relationships.

4.5. A discrepancy between Δ_{18} temperatures and previous estimates of the amount of thermogenic gas in the Antrim Shale?

Although the model describes the observed trends in both the isotopic and compositional parameters, it contrasts with previous studies in that it requires a larger thermogenic contribution (20 to 80% thermogenic) to gases from the northern margin of the Antrim Shale (Table 5) than previously proposed (<20%; Martini et al., 1996, 1998, 2003). It is important to consider that the values in Table 5 are modeled results and depend on the assumed Δ_{18} and δD_{CH4} value of the thermogenic end member, with higher Δ_{18}-based temperatures and/or more depleted δD_{CH4} values resulting in lower required amounts of the thermogenic component or vice-versa. For example, choosing the formation temperature for the thermogenic end member to be the maximum Δ_{18} temperature observed, 115 °C, changes the average thermogenic content of the gases to 50% (±28%, 1σ). Regardless, the higher-than-expected proportions of thermogenic gas (>20%) for some samples are an inescapable conclusion of the Δ_{18} temperatures: Even if the thermogenic component gases formed at infinite temperatures ($\Delta_{18} = 0$), mixing with a low temperature (~20 °C) gas would result in the average Δ_{18} temperature for the northern margin gases measured here, 67 °C, to be 25% thermogenic.

Furthermore, the maximum amount of C_{2-4} relative to C_{1-4} alkanes measured in the northern margin gases supports a higher-than-expected proportion of thermogenic gases. Specifically, in the northern margin, C_{2-4} alkanes can represent up to ~10% of all C_{1-4} alkanes (Table 3). If all gases were >80% biogenic, then the original thermogenic end member would need to be at least 50% C_{2-4} (assuming

Table 4
Thermogenic and biogenic end member values for mixing calculation

	Thermogenic end member	Biogenic end member
δD_{CH4} (‰)	−207[a]	−260[b]
$\delta^{13}C_{CH4}$ (‰)	−55[c]	−46[c]
$\delta D_{H2O,liquid}$ (‰)[d]	−11[e]	−102[f]
Δ_{18}-based T (°C)	144[g]	18[h]
C_1/C_{2-4}	5.8[i]	∞[j]

[a] *Source:* Maximum value of northern margin gases from the Antrim Shale (Martini et al., 2003).
[b] *Source:* Minimum value of northern margin gases from the Antrim Shale (Martini et al., 1998).
[c] *Source:* As discussed in the text.
[d] Maximum and minimum $\delta D_{H2O,liquid}$ were taken from units within the Antrim Shale, but outside of the northern margin. We have used samples from outside of the northern margin due to the large degree of fluid migration and mixing in the Michigan Basin (Wilson and Long, 1993; Martini et al., 1996, 1998; McIntosh and Walter, 2005), which lessens then chance of observing end-member compositions in the northern margin.
[e] *Source:* Maximum value of formation waters within the Antrim Shale (Wilson and Long, 1993). Specifically from the Berea Sandstone.
[f] *Source:* Minimum value of formation waters in the Antrim Shale (Martini et al., 2003). Specifically from the western margin.
[g] *Source:* Estimated as discussed in the text.
[h] *Source:* Average temperature of wells measured in this study (Table 3).
[i] *Source:* Average value for thermogenic gases from the central basin of the Antrim Shale and from Silurian formation gases (Martini et al., 1998, 2003).
[j] Biogenic gases are assumed to generate pure methane.

Table 5
Modeled relative concentrations of biogenic gas in Antrim Shale samples

Sample	Proportion of biogenic gas (%)	±[a] (%)
Butcher C3-24	75	6.1
Lake Horicon D4-15	49	1.5
Marlatt 1-7	66	8.9
North Charlton A1-18	77	4.1
State Charlton C4-18	44	0.1
State Charlton C4-31	65	3.4
State Loud B4-28	26	6.4
State Loud C2-31	18	0.2
State Charlton A3-32	54	7.8
Weber A4-10	75	8.4

[a] Errors are derived by propagating the 1σ errors of the Δ_{18} values of the samples through the calculation. They do not include the potential errors associated with our estimates of the end-member compositions.

pure mixing without oxidation, which only compounds the problem). However, C_{2-4} abundances relative to total C_{1-4} abundances of thermogenic gases in the Michigan Basin range from 10-30%, with an average of 15% (Martini et al., 1998, 2003). A higher relative concentration of thermogenic vs. biogenic gases would lower the necessary C_{2-4}/C_{1-4} value of the end member, bringing it closer to observed values in the Michigan Basin.

Thus, a significant question is why the original estimate for the amount of thermogenic relative to biogenic gas differs from those based on the constraints provided by the Δ_{18} temperatures and δD_{CH4} values in the mixing/oxidation model. The previous estimation was based on the linear relationship observed between δD_{CH4} and δD_{H2O}. Because this slope was similar to those observed in some natural settings dominated by hydrogenotrophic methanogens (e.g., Schoell, 1980), it was assumed that most of the gases were biogenic in origin, with a minor thermogenic component included to accommodate the presence of C_{2+} alkanes. This is a straightforward interpretation of the cause of the relationship between δD_{CH4} and δD_{H2O}. However, this relationship is not unique and can also be interpreted as a mixing line as above. When the additional constraints provided by the C_{1-4} concentrations and Δ_{18} temperatures are also included in the analysis, significant proportions of thermogenic gases become required in many of the samples. We stress that despite this greater-than-expected proportion of thermogenic gas in the samples, the Δ_{18} values indicate that biogenic gases also represent a significant, and in many cases dominant proportion of gases in the Antrim Shale (Table 5; Martini et al., 1996, 1998, 2003).

4.6. Potential implications of measured Δ_{18} values and the mixing/oxidation model for the generation and source of hydrocarbon gases in the Antrim Shale

If this mixing/oxidation model is correct, it has significant implications for the history of gas generation and migration in the Antrim Shale. Specifically, the formation temperature of the thermogenic component is, at a minimum, 115 °C, and, as modeled here, ~140 °C. The northern margin of the Antrim Shale, based on vitrinite reflectance data (R_0 between 0.4 and 0.6%; Cercone and Pollack, 1991) has remained below ~60 °C (Hunt, 1996). The Δ_{18} temperatures, therefore, demonstrate that the thermogenic components are unlikely to be locally sourced. Formations that could have reached these elevated temperatures include (i) the Antrim Shale in the central basin, which has vitrinite reflectance values as high as 1.0% (Martini et al., 2003), consistent with maximum temperatures of ~160 °C (Hunt, 1996); and (ii) more deeply buried Silurian and older strata underlying the Antrim Shale, that likely reached maximum burial temperatures above 100 °C (Cercone and Pollack, 1991) to 150 °C (Luczaj et al., 2006).

An additional constraint on the origin of the thermogenic gases in the northern margin is the predicted minimum δD_{CH4} value of −207‰ for the thermogenic component. This value may eliminate the central basin of the Antrim Shale as a potential source because gases there exhibit δD_{CH4} values between −270‰ to −280‰, though only two gases have been measured (Martini et al., 2003). Silurian-aged (or older) thermogenic gases derived from below the Antrim Shale are also plausible sources: stratigraphically equivalent formations from the Appalachian Basin in other Devonian, Silurian, and Ordovician aged formations commonly contain methane with δD values greater than −200‰ (Osborn and McIntosh, 2010).

Large scale mixing of gases from deeper portions of the basin, whether from the Antrim Shale or other units, could be reflected not only in the hydrocarbon composition of the gases, but in the chemical and isotopic compositions of the co-produced waters. This is because mixing of biogenic and thermogenic gases may and perhaps should co-occur with mixing of deeper basinal brines, which carry thermogenic gas, and fresher surficial waters, which contain biogenic gas. This prediction is borne out: the Δ_{18}-based temperatures correlate strongly with the δD values of the co-produced waters (Fig. 2f), with hotter temperatures correlating to enriched δD_{H2O} values. As demonstrated by Wilson and Long (1993) and Martini et al. (1998), δD_{H2O} values of waters in the Michigan Basin and northern margin of the Antrim Shale correlate with the salt composition of the waters. Specifically, more depleted δD_{H2O} values correlate with a low salt, meteoric water end member while more enriched δD_{H2O} values correspond to waters with a higher salt content. Wilson and Long (1993) and Martini et al. (1998) interpreted this relationship to indicate the mixing of basinal brines with meteoric water in the Michigan Basin, which is consistent with hydrological models of the Michigan Basin (e.g., McIntosh et al., 2011) and tracer studies using radiogenic isotopes (e.g., Ma et al., 2005). Thus, the relationship between Δ_{18} temperatures and δD_{H2O} values is consistent with previous geological, geochemical, and hydrological studies of Michigan Basin fluids and demonstrates the importance of interpreting clumped-isotope compositions of gases in both an environmental and geological context.

In summary, our finding of relatively high apparent temperatures for methane in Antrim Shale gases leads to two key conclusions: (i) there is more thermogenic gas in the system than previously proposed and (ii) that thermogenic component of the gas is probably derived from depth (from the basin center or below the northern margin of the Antrim Shale) and migrated to the shallow depths the Antrim Shale currently occupies on the basin rim. This is significant because the Antrim Shale is considered an end member of unconventional gas reservoirs in which the vast majority of gas formed *in situ* via microbial methanogenesis (Curtis, 2002) with the thermogenic component largely sidelined in subsequent interpretations. We interpret the Δ_{18} temperatures to indicate a different story: the biogenic gases are indeed derived *in situ* and represent ~50% of the gas. However the thermogenic component is an important contributor to the system (also ~50%) and formed elsewhere, mixing with the biogenic gas via migration. Thus the northern margin of the Antrim Shale can be considered a pseudo unconventional system—about half of the gas formed *in situ* while the other half formed elsewhere and migrated to the shale. Thus care should be taken in the use of the Antrim Shale as the type model for biogenic natural gas deposits (Curtis, 2002). Additionally, the importance of the relative amounts of biogenic and thermogenic gases in the Antrim Shale should factor into future calculations that suggest such deposits are major contributors of methane to the inventory of greenhouse gases in the atmosphere (Formolo et al., 2008). This alternative conclusion demonstrates the potential of Δ_{18} temperatures in untangling and quantifying the sources of gas to economically important gas reservoirs.

5. THE MEANING OF Δ_{18} TEMPERATURES FOR NATURALLY OCCURRING BIOGENIC SAMPLES

In the Antrim Shale, samples that yielded the lowest Δ_{18} temperatures have properties consistent with a dominantly biogenic origin. Similarly low Δ_{18} temperatures for biological samples were previously observed in biogenic methane derived from biodegraded oils in the Gulf of Mexico (Stolper et al., 2014b) and other sedimentary systems (Wang et al., in press). A simple interpretation of these measurements is that, in these environments, methanogens generate methane in or close to internal isotopic equilibrium. Two key questions brought up by these results are: (i) what are the driving biochemical reasons that biogenic methane in many natural settings are near internal isotopic equilibrium; and (ii) how common is this result and is it dependent on the environmental setting. To probe these questions, and thus help inform our interpretation of the measured composition of the Antrim biogenic component, we additionally measured methane created by methanogens from low-temperature seep environments (Santa Barbara and Santa Monica Basins), a pond from the Caltech campus, and methane generated by methanogens in pure-culture incubations (Tables 6 and 7, Fig. 5).

Methane samples from Santa Barbara and Santa Monica Basins yield Δ_{18}-based temperatures from 6 to 16 °C (Table 6) and are within 2σ error in all cases of their present bottom-water temperatures (5 to 9 °C; Table 6). We consider these samples to be nearly pure biogenic gas because they have low $\delta^{13}C$ values (−66‰ to −70‰), generally indicative of microbially derived methane (Whiticar, 1999), and are nearly pure methane (>99.5%).

In contrast, the pond sample yielded a negative Δ_{18} value (Fig. 5; Table 6), which is not thermodynamically possible for any sample in internal isotopic equilibrium at any temperature. This sample demonstrates that natural biogenic methane can yield Δ_{18} values strongly out of equilibrium. Data from laboratory cultures confirm this observation: all methane from cultured methanogens yield Δ_{18} values that differ from those predicted by their known growth temperatures, and also yield, in some cases, samples with negative Δ_{18} values (Table 7, Fig. 5). As discussed above, that such disequilibrium can occur was previously discussed and demonstrated in Stolper et al. (2014b) and presented in preliminary reports by this group (Stolper et al., 2014c; Eiler et al., 2014b) and preliminary reports by others (Gruen et al., 2014). Such observations have also recently been confirmed by Wang et al. (in press).

The interpretation of Δ_{18} values for methane from pure culture experiments is ambiguous because the observed disequilibrium could result from several different processes. For example, production of methane with continuously changing δD and $\delta^{13}C$ values due to Rayleigh distillation or changes in isotopic fractionation factors (Valentine et al., 2004), even if Δ_{18} values represented internal isotopic equilibrium, could result in disequilibrium Δ_{18} values due to the potential non-linear mixing effects on Δ_{18} values (Eiler

Table 6
Environmental biogenic samples

Sample Name	Lat	Long	Environmental T (°C)	Depth (m)	δD (‰)[a]	±[b]	$\delta^{13}C$ (‰)[c]	±[b]	Δ_{18} (‰)	±[b]	$T_{\Delta 18}$ (°C)[d]	±[b]	$\%CH_4$	$\%C_2H_6$	$\%CO_2$	n
J2-737 Santa Monica Basin	33.6397	−118.8007	5.2	897	−181.8	0.12	−70.4	0.01	6.46	0.27	16	8	99.80	0.01	0.19	1
J2-738 Santa Monica Basin	33.7992	−118.6470	5.3	500	−180.6	0.02	−70.2	0.05	6.8	0.12	8	3	99.89	0.01	0.11	2
J2-744 Santa Barbara Basin	34.3962	−120.1483	9.2	230	−179.2	0.12	−67.0	0.01	6.85	0.28	6	8	99.59	0.02	0.38	1
J2-749 Santa Monica Basin	33.6966	−119.0536	6.0	566	−169.5	0.10	−66.7	0.01	6.52	0.27	15	8	99.93	0.93	0.03	1
Caltech Pond	34.1386	−118.1255	20	<2	−319.5	0.11	−61.2	0.01	−1.01	0.29	–		–	–	–	1

[a] Referenced to VSMOW.
[b] If $n = 1$, ± errors are the standard deviation of a single measurement. If $n = 2$, ± errors are the standard error of the mean of the replicates.
[c] Referenced to the VPDB scale.
[d] Δ_{18}-based temperature.

and Schauble, 2004; Eiler, 2007, 2013; Stolper et al., 2014a,b). Alternatively, kinetic isotope effects during methane generation could create disequilibrium Δ_{18} values. It is thus significant that methane from a natural setting also exhibits a disequilibrium Δ_{18} value, indicating that such effects cannot be due solely to culturing artifacts.

5.1. Comparison of Δ_{18} temperatures to the δD_{CH4}-$\delta D_{H2O,liquid}$ heterogeneous phase geothermometer

Other geothermometers can be used to calculate 'apparent equilibrium temperatures' (Zhang, 1994) of methane formation. For example, equilibrium D/H fractionations between methane and water (i.e., $\alpha_{CH4–H2O,liquid}$) are a function of temperature (Bottinga, 1969; Richet et al., 1977; Horibe and Craig, 1995). We calculated the departure of $\alpha_{CH4–H2O,liquid}$ from the expected value for equilibrium at the given environmental or experimental temperature as discussed in the methods section above (Section 3.4). This departure is given by the quantity, ([measured $\alpha_{CH4–H2O,liquid}$]/[predicted equilibrium $\alpha_{CH4–H2O,liquid}$] − 1) × 1000. We also calculated departure from equilibrium for Δ_{18} values as ([measured $^{18}R/^{18}R^*$]/[predicted equilibrium $^{18}R/^{18}R^*$] − 1) × 1000. As given in equation 1, $^{18}R/^{18}R^*$ is ($\Delta_{18}/1000 + 1$) and is analogous to $\alpha_{CH4–H2O}$, except it is for a single phase.

The departure from equilibrium in Δ_{18} and $\alpha_{CH4–H2O,liquid}$ are compared in Fig. 6. In this figure, a value of 0‰ indicates that the measured quantity is identical to that expected for isotopic equilibrium. The origin, therefore, represents methane that is both in internal isotopic equilibrium and in hydrogen-isotopic equilibrium with water. Two key observations can be made about the data plotted in Fig. 6: (i) there are multiple points that plot in and around the origin, representing samples in equilibrium. And (ii) the degree of disequilibrium in Δ_{18} is correlated with that in $\alpha_{CH4–H2O,liquid}$. Put another way, disequilibrium in isotopic clumping appears to be related to disequilibrium in bulk D/H compositions. As discussed, above this relationship was first identified by Stolper et al. (2014c) and has recently been confirmed by Wang et al. (in press).

A simple interpretation of this data array is that when biogenic methane is in internal isotopic equilibrium (and Δ_{18} values yield sensible temperatures), it is in isotopic equilibrium with its source waters and plots at the origin of Fig. 6. This was not an unforeseen result—we expect that it is unlikely at relatively low (<100 °C) temperatures that methane is capable of exchanging hydrogen solely with itself in order to attain internal isotopic equilibrium. Instead methane presumably exchanges hydrogen with some other phase in order to be in internal isotopic equilibrium. Although there are multiple sources of reduced H that are used by methanogens to reduce CO_2 to CH_4 (Thauer, 1998), it is generally assumed, based on many experimental results, that these hydrogen species are in rapid isotopic equilibrium with hydrogen in water and thus that the D/H ratio of water ultimately controls the D/H ratio of methane (Daniels et al., 1980; Schoell, 1980; Balabane et al., 1987; Sugimoto and Wada, 1995; Whiticar, 1999; Valentine et al., 2004; Yoshioka et al.,

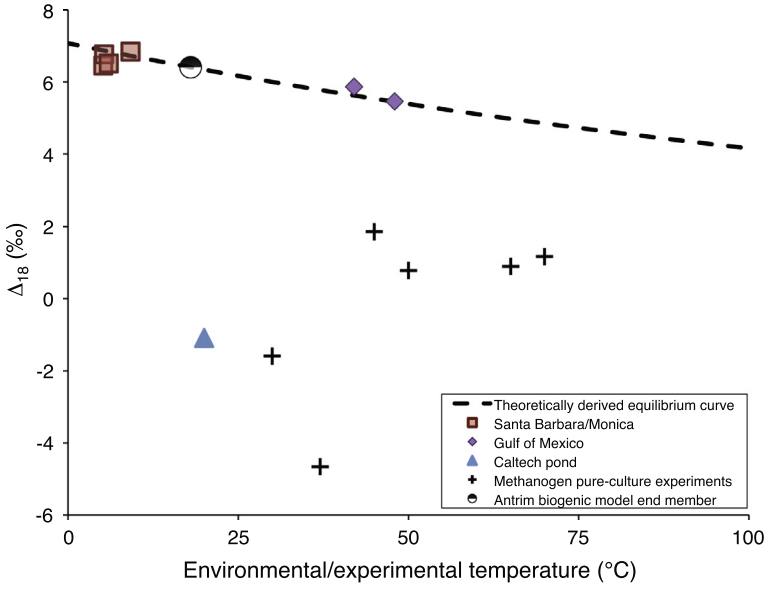

Fig. 5. Measured or modeled Δ_{18} values of biogenic gases from natural or experimental systems. The theoretically derived curve describes the expected Δ_{18} value for methane isotopically equilibrated internally as a function of temperature and is from Stolper et al. (2014a). The Gulf of Mexico samples were reported in Stolper et al. (2014b). The Antrim biogenic model end-member point is the value used in the mixing model of the Antrim Shale samples to describe the biogenic end member and is thus required to be on the equilibrium curve.

Table 7
Pure-culture experiments.

Species	Growth T (°C)	δD (‰)[a]	±[b]	$\delta^{13}C$ (‰)[c]	±[b]	Δ_{18} (‰)	±[b]
M. marburgensis	70	−317.2	0.12	−54.7	0.01	1.16	0.25
M. marburgensis	65	−367.3	0.11	−44.7	0.01	0.89	0.27
M. marburgensis	50	−356.7	0.12	−40.1	0.01	0.78	0.26
M. marburgensis	45	−317.9	0.1	−48.1	0.01	1.85	0.29
M. marburgensis	30	−476.0	0.1	−65.1	0.01	−1.59	0.25
M. barkeri	37	−491.6	0.12	−56.7	0.01	−4.66	0.26

[a] Referenced to VSMOW.
[b] Errors are the standard deviation of a single measurement as all samples were only measured once.
[c] Referenced to the VPDB scale.

2008). Therefore, it may not be surprising that the Δ_{18} values and $\alpha_{CH4-H2O,liquid}$ are related. This is discussed in more detail in the Appendix (specifically A2).

We note that there is scatter around the origin in Fig. 6, the point of mutual isotopic equilibrium between CH_4 and H_2O and internal isotopic equilibrium in CH_4. This could result from the fact that the hydrogen isotopic composition of cellular waters, which actually controls the value of δD_{CH4}, are not necessarily equivalent to the isotopic composition of the environmental waters (e.g., Kreuzer-Martin et al., 2005) or that our estimates for the $\delta D_{H2O,liquid}$ for the environmental pore waters (e.g., we assume the $\delta D_{H2O,liquid}$ value is 0‰ for all marine systems) is incorrect. A similar comparison for $\delta^{13}C$ values is not possible because $\delta^{13}C$ values of dissolved inorganic carbon or CO_2 were not measured for any samples and are difficult to estimate for the environmental samples as they can vary strongly (up to ~40‰) in sedimentary systems (Claypool and Kaplan, 1974).

5.2. An isotopic model of methanogenesis

To explore the relationship indicated by Fig. 6, we created a model for kinetic and equilibrium isotope effects associated with microbial methanogenesis. This model follows the mathematical framework introduced by Rees (1973) to describe the bulk isotopic composition of sulfide generated by sulfate-reducing bacteria and is influenced by the ideas presented in Blair (1998), Valentine et al. (2004), and Penning et al. (2005) that hypothesized and provided evidence that the bulk isotopic composition of methane is controlled in part by the overall reversibility of the enzymes involved in methanogenesis. The model also follows the initial ideas raised in Stolper et al. (2014b) that the reversibility of these enzymes also controls the clumped isotopic composition of methane. A full derivation of the model and assumptions implicit to it are given in the Appendix and follows the initial work presented by Eiler et al. (2014b). The model is similar in structure to that

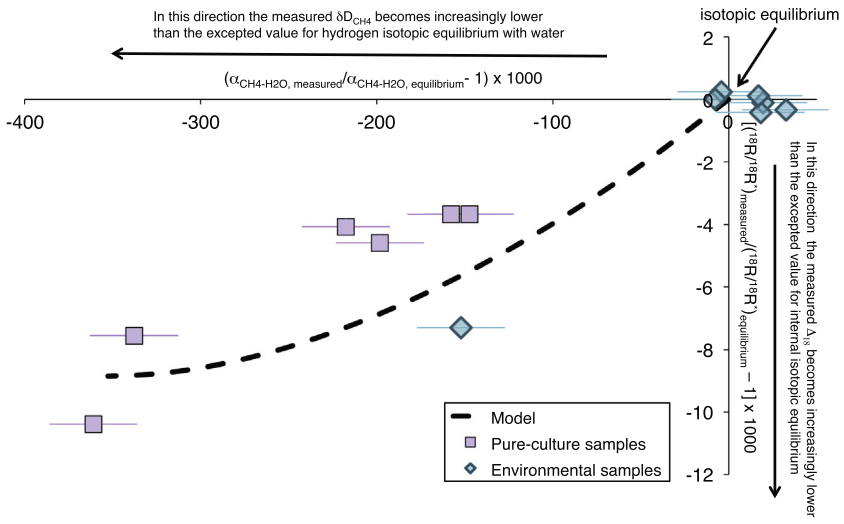

Fig. 6. Comparison of measured Δ_{18} values to those expected if the methane formed in internal isotopic equilibrium vs. the difference in measured δD_{CH4} and $\delta D_{H2O,liquid}$ values (expressed as a difference in ratios, $\alpha_{CH4-H2O,liquid}$) compared to that expected for heterogeneous phase isotopic equilibrium. Deviations in measured Δ_{18} values vs. those expected for equilibrium are represented in this figure through the comparison of $^{18}R/^{18}R^*$ values. As given in Eq. (1), $^{18}R/^{18}R^* = (\Delta_{18}/1000 + 1)$. All samples near the origin, which is the point at which methane is both internally isotopically equilibrated amongst all isotopologues and isotopically equilibrated for hydrogen isotopes with H_2O are from marine samples and assumed to have a $\delta D_{H2O,liquid} = 0‰$. The Caltech pond sample, the only environmental sample not located near the origin, was measured to have a $\delta D_{H2O,liquid}$ of $-16‰$. One pure-culture sample (the 65 °C experiment) was measured to have a $\delta D_{H2O,liquid} = -37.8‰$ for the culture media. We assume that this value is the same for all pure-culture experiments. We assume a conservative error for assignment of $\delta D_{H2O,liquid}$ of 25‰ to account for our estimations and potential for differences in the $\delta D_{H2O,liquid}$ of the environmental waters vs. the intracellular waters of the methanogens. The model describes the isotopic composition of methane formed by methanogens as a function of the reversibility of methyl-coenzyme M reductase. It is described in the text and Appendix.

recently proposed by Yoshinaga et al. (2014) for anaerobic methane oxidation and, as discussed above, Wang et al. (in press) for methanogenesis.

Three key assumptions are made in the model: (i) following the 'differential reversibility' hypothesis of Valentine et al. (2004), we assume that all metabolic intermediates between CO_2 and H_2 and a methyl group bound to a co-factor are in isotopic equilibrium (Fig. A3). (ii) We assume that H_2 and thus all methane precursors are in isotopic equilibrium with cellular H_2O (Valentine et al., 2004). (iii) We assign the rate-limiting step in methane production to be the final hydrogenation step catalyzed by methyl-coenzyme M reductase (MCR; Fig. A3). We note that the validity of the assumption (i), that all metabolic intermediates between the methyl group and CO_2 and H_2 are in isotopic equilibrium, is most valid for natural environments in which H_2 partial pressures are low and where there is a relatively small chemical potential contrast between the reactants and products of methanogenesis; however, as discussed in Valentine et al. (2004), in pure culture experiments where these chemical potential gradients are large, the metabolic intermediates may not be in isotopic equilibrium with CO_2 and H_2. In such a case, prior steps before MCR may be rate limiting. We discus this in more detail below in Section 5.4 after the description of the model.

In the model, we vary the degree of reversibility of MCR to explore whether the trend seen in Fig. 6 can be reproduced (Fig. A3). The capacity for MCR to catalyze both the addition and removal of a hydrogen from methane, i.e. that it is reversible, has been demonstrated using isotopic labeling techniques on MCR from the methanogen *M. marburgensis* (Scheller et al., 2010). Moreover, the capacity of anaerobic methanotrophs to synthesize MCR has led to the hypothesis that these organisms use the enzymes of methanogenesis (starting with MCR) in reverse to consume methane (e.g., Hallam et al., 2004; Thauer, 2011).

The required inputs for the model are given in Table 8. Rate constants are given in this table for individual

Table 8
Constants used for methanogenesis model.

Isotopologue ratio	κ_f[a,b]	α[c]	K_{eq}[d]
$^{13}CH_4/^{12}CH_4$	0.92 (0.92)	0.932	–
$^{12}CH_3D/^{12}CH_4$	2.112 (0.528)	0.816	–
$^{13}CH_3D/^{12}CH_4$	1.935	–	1.0061
$^{12}CH_2D_2/^{12}CH_4$	1.89	–	1.022

[a] Ratio of rate constants that describes the relative rate of formation of the two isotopologues from a methyl precursor.
[b] If a value is given inside a parenthetical, it refers to the equivalent bulk isotopic fractionation factor (α), which has been adjusted to take into the symmetry numbers of the isotopologues.
[c] Fractionation factor for isotopic equilibrium at 20 °C between CH_4 and CO_2 for $^{13}C/^{12}C$ ratios and between CH_4 and H_2O for D/H ratios.
[d] Equilibrium constant for internal equilibrium amongst all isotopologues for the indicated multiply substituted isotopologue (normalized against the equilibrium constant for a random distribution of isotopologues).

isotopologues. When a rate constant directly constrains a specific bulk fractionation factor between two phases (α), α is given as well. In the model, when MCR is assumed to be completely reversible, CH_4 is required to be in isotopic equilibrium with CO_2 and H_2O. The equilibrium isotopic fractionations between CH_4 and H_2O and CO_2 were calculated using $\alpha_{CH4-H2O,liquid}$ as described above and $\alpha_{CH4-CO2}$ values derived from Richet et al. (1977; Table 2). For the model, we assume an average temperature of 20 °C. Because the data in Fig. 6 come from a variety of different environments and environmental temperatures, this is clearly an approximation. However, the purpose of the model is to gain first-order insight into the meaning of Δ_{18} values observed in biogenic samples, and thus we consider this approximation to be acceptable for the time being. We calculated the equilibrium constants for homogeneous phase internal isotopic equilibrium between $^{13}CH_3D$ and $^{12}CH_2D_2$ with all other methane isotopologues (see Appendix) using the statistical mechanical model described in Stolper et al. (2014a).

In the model, when the rate of methane production exceeds that of consumption (through the reversal of MCR), a kinetic isotope effect can be expressed. We assume that the maximum kinetic hydrogen isotope effect ($\alpha_{CH4-H2O,liquid}$) is 0.528. This value is based on data from our study and is similar in magnitude to that found by pure-culture experiments on hydrogenotrophic methanogens from Balabane et al. (1987), 0.567. For the maximum kinetic carbon isotope $\alpha_{CH4-CO2}$, we assume a value of 0.92. This is intermediate to the maximum value observed in pure-culture experiments (0.93; Botz et al., 1996; Conrad, 2005), and from natural settings (up to 0.91; Whiticar, 1999). These values are fixed in the model. We then varied the rate constants for the kinetic isotope effect for $^{13}CH_3D$ and $^{12}CH_2D_2$ formation relative to $^{12}CH_4$ (Table 8) to achieve a best fit to the empirical data (Fig. 6). To first order, the relationship observed between $\alpha_{CH4-H2O,liquid}$ and Δ_{18} can be reproduced by our model.

5.3. Testing the model

The structure of our model and simple trend of the data in Fig. 6 make it clear that some combination of rate constants for the formation of $^{13}CH_3D$ and $^{12}CH_2D_2$ relative to $^{12}CH_4$ will provide an adequate fit to the data. Nevertheless, the basic validity of the model can be tested by examining whether the required rate constants for $^{13}CH_3D$ and $^{12}CH_2D_2$ relative to $^{12}CH_4$ formation are chemically realistic. Thus we compared the isotope effects of ^{13}C and D addition to singly substituted isotopologue precursors to the primary isotope effects prescribed by the model (e.g., Bigeleisen and Wolfsberg, 1958). For example, the fitted relative difference in the rate constants for $^{13}CH_3D$ vs. $^{12}CH_3D$ formation is 0.916. This is similar to the prescribed value for the relative rates of $^{13}CH_4$ vs. $^{12}CH_4$ formation, 0.92. Similarly, the relative formation rates for $^{12}CH_2D_2$ vs. $^{12}CH_3D$ (normalized for the symmetry numbers of the different isotopologues) were modeled to have a value of 0.6. Again, this is similar to the value used for the rate of $^{12}CH_3D$ formation relative to $^{12}CH_4$ (again normalized for symmetry numbers), 0.528. The modeled rate constants for $^{13}CH_3D$ and $^{12}CH_2D_2$ formation relative to $^{12}CH_4$ are thus chemically reasonable, and quite similar to the isotope effects required for a single ^{13}C or D substitution. Such a coincidence was not a forgone conclusion, and helps to demonstrate the self-consistency of our model. Furthermore, the model is testable through the independent measurement of the abundances of $^{13}CH_3D$ and $^{12}CH_2D_2$ because only specific trends, based on this model, are allowed (Fig. 7). I.e., if their abundances can be measured independently this model can be tested explicitly (preliminary results for such measurements were presented by Eiler et al., 2014b).

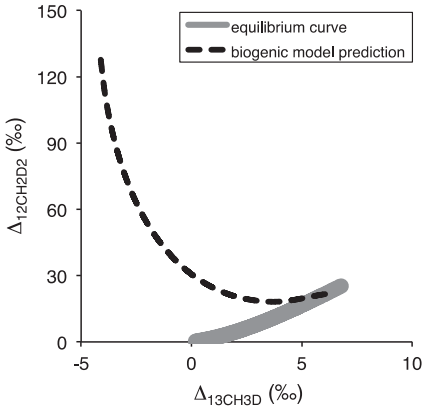

Fig. 7. Comparison of the biogenic model (described in the text) vs. the expected values for internal isotopic equilibrium for $\Delta_{12CH2D2}$ and Δ_{13CH3D} values. $\Delta_{12CH2D2} = [([^{12}CH_2D_2]/[^{12}CH_4])/([^{12}CH_2D_2]^*/[^{12}CH_4]^*) - 1] \times 1000$. $\Delta_{13CH3D} = [([^{13}CH_3D]/[^{12}CH_4])/([^{13}CH_3D]^*/[^{12}CH_4]^*) - 1]$. * refers to the random isotopic distribution. If both Δ_{12H2D2} and Δ_{13CH3D} can be measured, the model can be tested.

5.4. Model considerations

The analysis above indicates that the model is plausible, makes testable predictions, and is consistent with the observed data (Fig. 6). However, the model makes several simplifications that we consider more closely here:

(1) The model assumes that the final step of methanogenesis, the hydrogenation of a methyl group catalyzed by MCR, is the rate-limiting step, and that all previous steps are in isotopic equilibrium. However, in some pure-culture experiments it is thought that under high hydrogen partial pressures (at least > 400 Pa as in the experiments here), prior steps in the generation of methane may be rate limiting (Valentine et al., 2004; Penning et al., 2005) such that CO_2 in the growth medium is not in isotopic equilibrium with the metabolic intermediates. This is sometimes evidenced by relatively small carbon isotope fractionation factors between methane and CO_2—for example $\alpha_{CH4-CO2}$ values range from 0.927 to 0.976 in pure-culture experiments (Valentine et al., 2004; Conrad, 2005).

As the model presented here assumes that MCR is the rate-limiting step and that all isotope effects are 'normal,' i.e., that products are always isotopically lighter than the reactants, it requires that $\alpha_{CH4-CO2}$ will be between 0.92 and 0.932. This indicates that for some pure-culture experiments, the model presented will be unlikely to fit the carbon isotope data. However, as we did not measure the $\delta^{13}C$ values of the CO_2 in our experiments nor in most of the environmental samples, it is difficult to evaluate whether this is an issue for the data presented here. A larger range of $\alpha_{CH4-CO2}$ can be modeled if steps prior to MCR are allowed to be rate limiting in some conditions. Though conceptually simple, incorporation of this step introduces up to 9 new and unconstrained variables: the reversibility of the step, two forward (or reverse) and two equilibrium isotope effects for bulk hydrogen and carbon isotopic compositions, and up to two forward (or reverse) and equilibrium isotope effects for clumping reactions between ^{13}C with D and D with D. In contrast to this model, Wang et al. (in press) present a model with 6 potentially rate-limiting steps, the diffusion of CO_2 into the cell, 4 hydrogenation steps, and the diffusion of CH_4 out of the cell. To reduce the number of unconstrained free variables in the model, they assume that CO_2 diffusion into the cell and CH_4 diffusion out of the cell are not isotopically discriminating steps, that CO_2 in the cell is in chemical equilibrium with CO_2 outside of the cell, that all hydrogenation steps for methane precursors (i.e., CO_2, R-CH, R-CH2, R-CH3, where R represents the molecule to which the carbon) have the same forward and reverse kinetic isotope effects for bulk carbon, bulk hydrogen, and clumped isotopic compositions (but with different values for bulk carbon-isotope vs. bulk hydrogen-isotope. vs. clumped-isotope effects), and that all hydrogenation steps have the same forward vs. reverse reaction rate, i.e., are equally reversible or irreversible. They predict that $\alpha_{CH4-CO2}$ values will be between 0.96 and 0.932, but do not present or discuss $\delta^{13}C$ measurements of CO_2 in their environmental samples vs. the prediction of the model. Future models could attempt to calculate or experimentally constrain the various isotope effects involved with all species intermediate to CH_4 and CO_2 and H_2. Additionally, a clear next step is to perform experiments and make measurements in natural systems in which the $\delta^{13}C_{CO2}$ value is monitored along with δD_{H2O}, δD_{CH4}, $\delta^{13}C_{CH4}$, and Δ_{18}.

(2) The model implicitly requires that isotopic equilibrium between CH_4 and both CO_2 and H_2O is reached at the same time. However, it is possible that MCR could catalyze exchange reactions more rapidly between CH_4 and H_2O than slower back reactions to CO_2. In this case, isotopic equilibrium between CH_4 and H_2O and, as a consequence, internal isotopic (i.e., Δ_{18}) equilibrium could be achieved without carbon-isotope equilibrium between CH_4 and CO_2. If so, a more complex model that allows different rates of isotopic exchange for H and C would be required, such as those used to describe the combined sulfur and oxygen isotope systematics of SO_4^{2-} during dissimilatory sulfate reduction (e.g., Brunner et al., 2005). This consideration raises a potentially interesting point related to possible effects on Δ_{18} values for anaerobic methane oxidation. It has recently been suggested, based on both experimental data and model constraints, that under low sulfate conditions (~1–2 mM sulfate) anaerobic methane oxidizers can nearly completely (80%) isotopically equilibrate methane with dissolved CO_2 (Yoshinaga et al., 2014). As discussed above, this process is thought to be catalyzed through operation of MCR in reverse (Hallam et al., 2004; Thauer, 2011), which itself, for the model of Yoshinaga et al. (2014), is up to 80% reversible. This then suggests that hydrogen-isotope-exchange reactions between CH_4 and H_2O should be at least as equilibrated if not more so than carbon isotopes between CH_4 and CO_2. Consequently, anaerobic methane oxidation could result in Δ_{18} values of residual methane that reflect the temperatures of methane oxidation at low sulfate levels. In such a scenario, the Δ_{18} values of gases from, for example, thermogenic systems, could potentially be reset to reflect lower temperatures of methane oxidation. This appears not to be the case in the Antrim Shale, indicating either limited amounts of anaerobic methane oxidation is occurring or that thermogenic gases are sorbed to shales or otherwise inaccessible to microbial communities living in fractures until active pumping in a well occurs.

(3) The model does not explicitly treat methylotrophic methanogenesis in which acetate or some other organic substrate (e.g. methanol or methylamine) is the precursor to methane. The Δ_{18} values of methane generated by this pathway, either in the lab or in nature, are unknown and will be important to constrain in future work. Nevertheless, we note that our pond sample likely contained aceticlastic methanogens, as they are commonly present in shallow, freshwater anoxic sediments (Whiticar et al., 1986), yet data from this sample are broadly consistent with the model. We speculate that – because aceticlastic methanogens also use MCR – our model may be more broadly generalizable.

Despite these model simplifications, the critical point is that clumped-isotope measurements from both culture-based and natural biogenic methane can be explained (Fig. 6) in the context of a simple, plausible, and testable (Fig. 7) model. Just as models to describe sulfate reduction in the context of isotopic measurements have evolved over the course of 40 years (Rees, 1973; Farquhar et al., 2003; Brunner and Bernasconi, 2005; Bradley et al., 2011; Wing and Halevy, 2014), we expect that more advanced and complex treatments of methanogenesis will address the issues presented above.

5.5. Implications for clumped-isotope thermometry of biogenic methane

Our model provides insight into the metabolic state of methanogens living in different environmental settings and is consistent with the, albeit limited, empirical data to-date (Fig. 6). For example, systems where low, environmentally plausible Δ_{18} temperatures have been observed are marine settings in the Santa Barbara and Santa Monica Basins, buried oil-degrading methanogenic communities in the Gulf of Mexico (Stolper et al., 2014b), and organisms buried in the Antrim Shale. In these, 'deep biosphere' systems and shallow marine settings, organic carbon has already been substantially degraded and even thermally altered before becoming available to methanogens and hydrogen partial pressures are likely very low (Burke, 1993). In such systems, growth and metabolic rates are slow compared to laboratory cultures of methanogens, and thus could allow internal isotopic equilibrium to be reached. For example, in the New Albany Shale, which is similar in age and depositional environment to the Antrim Shale, rates of methane generation are estimated based on accumulations of radiogenic ^{4}He to have been 10^4–10^6 slower than equivalent laboratory manipulations (Schlegel et al., 2011). In the context of the model, MCR would be almost entirely reversible in such settings and thus would generate methane in internal isotopic equilibrium. Additionally, this insight provides independent justification for the assumption that the methanogens in the Antrim Shale generate methane at internal isotopic equilibrium.

Fast metabolic rates in which methane is generated rapidly and MCR is not completely reversible would be expected to generate methane out of isotopic equilibrium. This is also consistent with current observations: In laboratory cultures, large partial pressures of hydrogen and CO_2 are used to stimulate growth and generate methane rapidly. In the Caltech pond, plant litter is continually deposited at the sediment water interface that has undergone limited biodegradation, potentially stimulating rapid methanogenesis.

Based on these considerations, we predict that systems in nature where growth rates are slow, such as in marine sediments and deeply buried (many meters) continental systems, methane will form in internal isotopic equilibrium. Shallow sediments in terrestrial systems, on the other hand, where methane generation rates are high, will yield methane out of equilibrium. More broadly, this analysis indicates that Δ_{18} values of biogenic methane potentially reflect the metabolic state of methanogens and thus can be used to probe growth and metabolic rates of methanogenesis in the environment.

Additionally, our model potentially explains a long-standing discrepancy between the δD values of methane observed in culture experiments vs. in some natural settings. Specifically, in many natural settings, especially marine sediments, differences between δD_{CH4} and $\delta D_{H2O,liquid}$ are significantly less (>100‰; Schoell, 1980; Whiticar et al., 1986; Burke, 1993) than observed in cultures (e.g., Balabane et al., 1987; Valentine et al., 2004; Yoshioka et al., 2008; Hattori et al., 2012) and natural systems such as cow rumens (e.g., Bilek et al., 2001) and freshwater soils (e.g., Sugimoto and Wada, 1995). Explanations for this difference have included the incorporation of H from H_2 into methane (Burke, 1993) and variability of isotopic fractionation (Valentine et al., 2004). Our model and the Δ_{18} values suggest an alternative, though not necessarily exclusive, explanation: specifically that in marine settings and 'deeply' buried continental systems isotopic equilibrium between methane and local waters is reached. This equilibrium results in an ~160–200‰ difference in δD between water and methane (Schoell, 1980; Whiticar et al., 1986). In contrast, in shallow, terrestrial systems, isotopic equilibrium is not reached and a larger kinetic isotope effect for D/H ratios of methane is expressed.

Finally, the model, as inspired by the work of Blair (1998), Valentine et al. (2004), and Penning et al. (2005) and building on the initial ideas of Stolper et al. (2014b), Stolper et al. (2014c), and Eiler et al. (2014b), demonstrates the importance of considering both kinetics and equilibrium thermodynamics in the consideration of the controls on the isotopic compositions of reactants and products not only in methanogenesis, but a range of other metabolisms. This is not a novel idea and has been long considered in the studies of dissimilatory sulfate reduction (Rees, 1973; Farquhar et al., 2003; Brunner and Bernasconi, 2005; Bradley et al., 2011; Wing and Halevy, 2014). However, the use of clumped-isotope measurements to study microbial metabolisms provides a new, distinct avenue for studying the flow of metabolites in the metabolism of organisms by providing a reference frame that is grounded in equilibrium thermodynamics and a fingerprint that remains with the molecule of interest even after separation from its formational environment.

6. CONCLUSIONS

We have demonstrated that clumped-isotope measurements of methane can be useful for quantifying the amount of biogenic vs. thermogenic methane in natural settings. In the Antrim Shale, significant quantities of both biogenic and thermogenic methane are present in different wells, with Δ_{18}-based temperatures correlating with other measured parameters such as C_1/C_{2-4} ratios, $\delta D_{H2O,liquid}$ and δD_{CH4}. The mixing model results show that, in contrast to previous indications, biogenic and thermogenic methane are approximately equal in importance in the northern margin of the Michigan basin. Additionally, the Antrim Shale results support previous findings that biogenic gases in natural systems frequently yield low Δ_{18} temperatures consistent with their formation environments. This was also observed in samples from offshore seeps of biogenic gas. However, a pond sample and pure-culture experiments yield Δ_{18} temperatures that are strongly inconsistent with the known environmental or experimental temperatures. We present a metabolically based model that explicitly considers the reversibility of enzymes in methanogenesis. This model predicts that when rates of methanogenesis are slow, environmentally consistent temperatures result from the internal equilibration of methane with its metabolic precursors while the unrealistic temperatures result from the

expression of kinetic isotope effects during rapid methane generation. Our model indicates that in many natural settings where methanogen growth rates are slow, such as in sedimentary basins and marine sediments, methane can be produced in or near isotopic equilibrium. By contrast, in settings that allow for high rates of methane generation such as ponds and near-surface environments, the methane is generated out of internal isotopic equilibrium. This potentially explains why methane from different environments can have drastically different D/H fractionations relative to water, and indicates that methanogens in many natural settings live near thermodynamic equilibrium, eking out a slow living.

ACKNOWLEDGEMENTS

The idea to measure clumped-isotope compositions of methane from the Antrim Shale resulted from a fortuitous meeting of DAS, JME, ALS, and AMM at the 2012 Gordon Research Conference on organic geochemistry. We wish to thank the conveners of that conference, Tim Eglinton and Erdem Idiz (and all other participants) for inviting us to the conference and creating a stimulating atmosphere for scientific discussion and collaboration. We additionally wish to thank Fenfang Wu for help measuring the δD of water from the culturing experiments, Jared Leadbetter for aid in sampling methane from the Caltech pond, and the crew of the *R/V Atlantis*. Finally, we would like to thank three anonymous reviewers and the associate editor, Ed Hornibrook, for their helpful comments. DAS was supported through the NSF GRFP. Research was supported by Caltech and an NSF EAR grant to JME, ACS, PRF grant to AMM, and NSF grants OCE-1046144, OCE-1155855 and EAR-0950600 to DLV and SSS.

APPENDIX A.

A.1. Derivation of isotopically enabled methanogenesis model

In this section we derive a model to describe the concentrations of various isotopologues of methane generated during microbial methanogenesis in order to calculate δD_{CH4}, $\delta^{13}C_{CH4}$, and Δ_{18} values. This model is based on the quantitative framework of Rees (1973) originally used to describe isotope fractionations of sulfur during dissmilatory sulfate reduction. We only deal with hydrogenotrophic methanogenesis here and do not incorporate aceticlastic or methylotrophic methanogenesis.

The generation of methane by methanogens involves many steps with 6 distinct metabolic intermediates between $CO_2 + H_2$ and CH_4 (Thauer, 1998). A full description of the isotopic fractionation factors of each individual step in both the forward and backward direction is desirable, and ultimately necessary for a complete description of the isotopic ratios observed for methane in nature. However, the individual fractionation factors for ^{13}C or D in the singly substituted isotopologues are not known for most steps, let alone for $^{13}CH_3D$ and $^{12}CH_2D_2$ (Scheller et al., 2013). We deal with this complexity by making a few simplifying assumptions regarding the metabolism of methanogens. We assume that the final step of methanogenesis in which a hydrogen atom is added to a methyl group attached to coenzyme M (CH_3-S-CoM) is the rate-limiting step, and

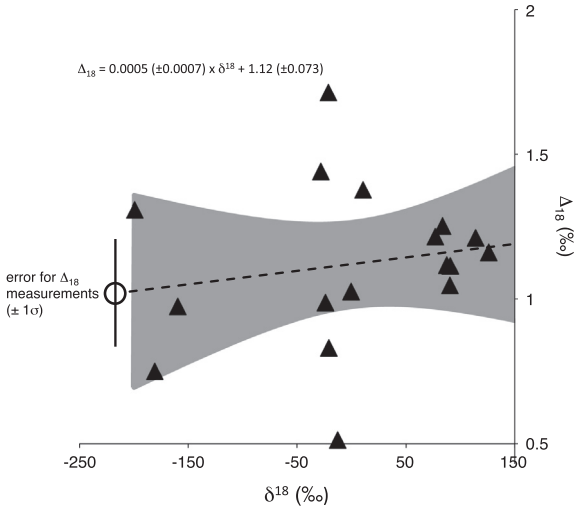

Fig. A1. Comparison of measured Δ_{18} values vs. the average isotopic composition (tracked via δ^{18} values) for gases equilibrated at 500 °C in the lab using nickel catalysts as described in Stolper et al. (2014a). The δ^{18} values are dominantly controlled by variations in the δD value of the gas. No statistically significant dependence for Δ_{18} on δ^{18} is observed: the slope is 0.0005‰ and the 1σ error of the slope is 0.0007‰. Additionally the intercept of the line, 1.12‰ (±0.073, 1σ), is within 1σ of the long-term average value for 500 °C heated gases, 1.06‰. The overall standard deviation of the measured points is 0.28‰, similar to the internal precision of each individual measurement (~0.25‰).

that this step proceeds sufficiently slowly compared to the previous steps that the precursor metabolites are in isotopic equilibrium (Fig. A3). This follows arguments made in Valentine et al. (2004) based on the 'differential reversibility' hypothesis put forward there and discussed in the text above. We additionally assume, following Botz et al. (1996), that only a small proportion of CO_2 is used for biomass generation (<10%; Fuchs et al., 1979) as compared to methane production and therefore can be, to first order, neglected in the model. We note though that *M. barkeri* belongs to an order of methanogens that have significantly (~2-3x) higher biomass yields than other orders (Thauer et al., 2008). This organism gave the most negative Δ_{18} value and may indicate that incorporation of biomass yields is important for understanding the isotopic composition of methane.

We can thus, in a simplified way, describe the overall generation of methane during methanogenesis with two reactions. The first reaction between CO_2 and CH_3-S-CoM:

$$CO_2 + 3H_2 + \text{H-S-CoM} \leftrightarrows CH_3\text{-S-CoM} + 2H_2O \quad (A1.1)$$

where all species are in isotopic equilibrium (Fig. A3). S-CoM represents coenzyme M. The two-headed arrows indicate that the different species are at chemical and isotopic equilibrium. The rate-limiting step (where reduced H is donated from a reduced hydrogen pool) is then:

$$CH_3\text{-S-CoM} + 2H \rightarrow CH_4 + \text{H-S-CoM}. \quad (A1.2)$$

In this derivation, the consequences of allowing equation A1.2 to proceed in the reverse direction will be explored.

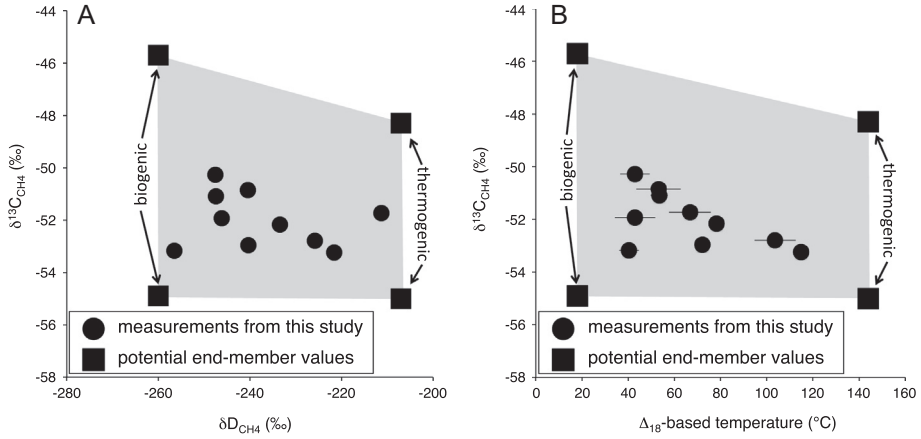

Fig. A2. Comparison of potential $\delta^{13}C_{CH4}$ values for the biogenic and thermogenic end members for the mixing model discussed in the main text for (A) $\delta^{13}C_{CH4}$ vs. δD_{CH4} and (B) $\delta^{13}C_{CH4}$ vs. Δ_{18}-based temperatures. The range of biogenic end members was taken from the maximum and minimum $\delta^{13}C_{CH4}$ values for gases from the northern margin of the Antrim Shale with $C_1/C_{2-4} > 500$. The maximum and minimum values are found in Martini et al. (1998). The thermogenic values were found by taking the maximum and minimum range of $\delta^{13}C_{CH4}$ values for gases from the Antrim Shale with $C_1/C_{2-4} < 100$, including those outside of the northern margin (Martini et al., 1998, 2003). Because the overall potential range of $\delta^{13}C_{CH4}$ values is far larger than the total range of $\delta^{13}C_{CH4}$ values observed in this study (3‰), the leverage that the $\delta^{13}C_{CH4}$ values provide for validating the model is low.

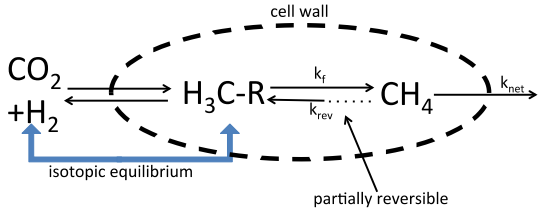

Fig. A3. Cartoon of the isotopically enabled model of methane formation described in the main text and Appendix. The dotted lines mark the boundary between the methanogen cell and extracellular water. In this model, CO_2 and H_2 are assumed to always be in isotopic equilibrium with a methyl group bound to coenzyme M (here symbolized with the 'R') following the differential reversibility hypothesis of Valentine et al. (2004). Additionally, the H_2 and hydrogen in the methyl group bound to coenzyme M are assumed to be in isotopic equilibrium with the intracellular H_2O. In the model, the reversibility of methyl-coenzyme M reductase (the relative rates of the steps symbolized by k_{rev} vs. k_f) is varied as discussed in the Appendix.

A.2. $^{13}CH_4$ Derivation

The set of equations that describe the dependence of the $^{13}CH_4/^{12}CH_4$ ratio on the degree of reversibility of equation (A1.2) are derived here for the following reactions:

$$^{12}CH_3\text{-S-CoM} + H \underset{^{12CH3}k_f}{\overset{^{12CH4}k_{rev}}{\leftrightarrows}} {}^{12}CH_4 \xrightarrow{^{12CH4}k_{net}} \quad \text{(A2.1)}$$

and

$$^{13}CH_3\text{-S-CoM} + H \underset{^{13CH3}k_f}{\overset{^{13CH4}k_{rev}}{\leftrightarrows}} {}^{13}CH_4 \xrightarrow{^{13CH4}k_{net}} \quad \text{(A2.2)}$$

Here, for clarity, we have left off the additional reaction in which H-S-CoM is regenerated as written in Eq. (A1.2). The rate constants describing each reaction are given next to the arrows for each step. The final step of the reaction in which methane leaves the system can be envisioned as diffusion or escape of methane out of the cell or environment such that it can no longer interact with the enzymes of the methanogens. It is assumed that all reactions follow the kinetic forms discussed in Rees (1973). Equations will only be developed for the system at steady state such that the concentrations of all metabolic intermediates are time invariant.

With this in mind, for the reaction in (A2.1),

$$\frac{d[^{12}CH_4]}{dt} = 0 = {}^{12CH_3}k_f[^{12}CH_3\text{-S-CoM}][H] - ({}^{12CH_4}k_{rev} + {}^{12CH_4}k_{net})[^{12}CH_4], \quad \text{(A2.3)}$$

such that, at steady state,

$$[^{12}CH_4] = \frac{{}^{12CH_3}k_f[^{12}CH_3\text{-S-CoM}][H]}{{}^{12CH_4}k_{rev} + {}^{12CH_4}k_{net}}. \quad \text{(A2.4)}$$

Brackets denote concentrations of the species. In writing the equations in this form, we assume there exists some pool of hydrogen (and deuterium) that is used for all reactions. Multiple enzymes donate H to methane precursors, and thus this assumption is not strictly correct (Thauer, 1998; Valentine et al., 2004). Here, we assume that all pools of hydrogen are isotopically equilibrated with water. This is generally assumed and supported by a variety of experiments and observations (Daniels et al., 1980; Schoell, 1980; Balabane et al., 1987; Sugimoto and Wada, 1995; Whiticar, 1999; Valentine et al., 2004; Yoshioka et al., 2008). However, we note this assumption has recently been questioned by Kawagucci et al. (2014). Their results suggest, as proposed by Burke (1993), that the isotopic composition of hydrogen from H_2, independent of the isotope composition of water, partially controls the isotopic

composition of the resultant methane. Regardless, we will proceed with the assumption that all hydrogen in methane is ultimately derived from water. Similarly, for Eq. (A2.2) we have,

$$[^{13}CH_4] = \frac{^{13CH_3}k_f[^{13}CH_3\text{-S-CoM}][H]}{^{13CH_4}k_{rev} + {}^{13CH_4}k_{net}}. \quad (A2.5)$$

An important approximation is used in Eqs. (A2.3)–(A2.5): a small proportion of methyl groups have a deuterium added instead of a hydrogen (as written). These deuterium addition reactions are ignored as they represent <0.1‰ of all methane groups generated for each reaction, which we consider an acceptable approximation.

Finally, we introduce here a 'degree of reversibility' term for Eq. (A2.1). This term, 'r', introduced by Rees (1973), compares the rate of back reaction of methane into the metabolic intermediates vs. the forward generation rate of methane. In the form of an equation,

$$r = \frac{^{12CH_4}k_{rev}[^{12}CH_4]}{^{12CH_3}k_f[^{12}CH_3\text{-S-CoM}][H]}. \quad (A2.6)$$

In this framework, r can vary from 0 to 1. Combination of (A2.6) with (A2.4) results in:

$$r = \frac{^{12CH_4}k_{rev}}{^{12CH_4}k_{rev} + {}^{12CH_4}k_{net}}. \quad (A2.7)$$

Division of (A2.5) by (A2.4) yields

$$\frac{[^{13}CH_4]}{[^{12}CH_4]} = \left(\frac{^{13CH_3}k_f[^{13}CH_3\text{-S-CoM}][H]}{^{12CH_3}k_f[^{12}CH_3\text{-S-CoM}][H]}\right) \times \left(\frac{^{12CH_4}k_{rev} + {}^{12CH_4}k_{net}}{^{13CH_4}k_{rev} + {}^{13CH_4}k_{net}}\right). \quad (A2.8)$$

This can be rewritten using the following notations:

$$^{13CH_4}R = \frac{[^{13}CH_4]}{[^{12}CH_4]} \text{ and } {}^{13CH_3}R = \frac{[^{13}CH_3\text{-S-CoM}]}{[^{12}CH_3\text{-S-CoM}]} \quad (A2.9a \text{ and } b)$$

and

$$^{i}\kappa_j = \frac{^{i}k_j}{^{\text{unsubstituted}}k_j}. \quad (A2.10)$$

'Unsubstituted' refers to an isotopologue without ^{13}C or D: i.e., $^{12}CH_3$-S-CoM or $^{12}CH_4$. Substituting Eqs. (A2.7), (A2.9) and (A2.10) into (A2.8) and assuming that there is no isotopic fractionation during the net removal of methane (i.e., $^{13CH4}\alpha_{net} = 1$) gives

$$^{13CH_4}R = {}^{13CH_3}R \times {}^{13CH_3}\kappa_f \times \left(\frac{1}{1 + r(^{13CH_4}\kappa_{rev} - 1)}\right). \quad (A2.11)$$

It is inconvenient to describe $^{13CH4}R$ in terms of $^{13CH3}R$ because $^{13CH3}R$ is not a measureable quantity. This term can be eliminated because it is assumed that in the system, at all times, all metabolites from CO_2 and H_2 through CH_3-S-CoM are in isotopic equilibrium. Thus we can write the following isotope-exchange reaction:

$$^{13}CO_2 + {}^{12}CH_3\text{-S-CoM} \leftrightarrows {}^{12}CO_2 + {}^{13}CH_3\text{-S-CoM}. \quad (A2.12)$$

The equilibrium constant for this reaction is:

$$K_{eq}_{^{13}CO_2 \leftrightarrows {}^{13}CH_3\text{-S-CoM}} = \frac{^{13CH_3}R}{^{13CO_2}R} \quad (A2.13)$$

where

$$^{13CO_2}R = \frac{[^{13}CO_2]}{[^{12}CO_2]}. \quad (A2.14)$$

Substituting (A2.13) into (A2.11) yields:

$$^{13CH_4}R = {}^{13CO_2}R \times K_{eq}_{^{13}CO_2 \leftrightarrows {}^{13}CH_3\text{-S-CoM}} \times {}^{13CH_3}\kappa_f \times \left(\frac{1}{1 + r(^{13CH_4}\kappa_{rev} - 1)}\right) \quad (A2.15)$$

We define a new term such that:

$$^{13CH_3}\kappa_f^* = K_{eq}_{^{13}CO_2 \leftrightarrows {}^{13}CH_3\text{-S-CoM}} \times {}^{13CH_3}\kappa_f. \quad (A2.16)$$

$^{13CH3}\kappa_f^*$ is thus not strictly a ratio of rate constants (as kinetic isotope effects are usually defined), but instead incorporates the equilibrium fractionation between CO_2 and CH_3-S-CoM and the rate-limiting step of hydrogen addition to CH_3-S-CoM. Such 'combined,' multi-step fractionation factors are commonly described in models of this sort as often only the product and reactants are measureable (Hayes, 2001). Regardless, substitution of (A2.16) into (A2.15) yields:

$$^{13CH_4}R = {}^{13CO_2}R \times {}^{13CH_3}\kappa_f^* \times \left(\frac{1}{1 + r(^{13CH_4}\kappa_{rev} - 1)}\right) \quad (A2.17)$$

When r = 1, CH_4 and CO_2 are in isotopic equilibrium (by definition). And we have:

$$\frac{^{13CH_4}R_{eq}}{^{13CO_2}R_{eq}} = \frac{^{13CH_3}\kappa_f^*}{^{13CH_4}\kappa_{rev}} \quad (A2.18)$$

where 'eq' signifies a value at isotopic equilibrium. We can write the following isotope-exchange reaction as well:

$$^{13}CO_2 + {}^{12}CH_4 \leftrightarrows {}^{12}CO_2 + {}^{13}CH_4. \quad (A2.19)$$

This reaction has the following equilibrium constant,

$$K_{eq}_{^{13}CO_2 \leftrightarrows {}^{13}CH_4} = \frac{^{13CH_4}R_{eq}}{^{13CO_2}R_{eq}}. \quad (A2.20)$$

Combination of (A2.20) with (A2.18) yields:

$$K_{eq}_{^{13}CO_2 \leftrightarrows {}^{13}CH_4} = \frac{^{13CH_3}\kappa_f^*}{^{13CH_4}\kappa_{rev}} \quad (A2.21)$$

This equilibrium constant is calculable using the theory of, for example, Richet et al. (1977). Thus, Eq. (A2.21) removes a degree of freedom from Eq. (A2.17).

A.3. $^{12}CH_3D$ derivation

The set of equations that describe the dependence of the $^{12}CH_3D/^{12}CH_4$ ratio on the degree of reversibility of Eq.

(A1.2) is derived in this section. The derivations, although similar to Section A2, have a fundamental difference related to the fact that $^{12}CH_3D$ can be made two different ways:

$$^{12}CH_3\text{-S-CoM} + D \underset{^{12+D}k_f}{\overset{^{12-D}k_{rev}}{\leftrightarrows}} {}^{12}CH_3D \overset{^{12CH3D}k_{net}}{\rightarrow} \quad (A3.1)$$

and

$$^{12}CH_2D\text{-S-CoM} + H \underset{^{12+H}k_f}{\overset{^{12-H}k_{rev}}{\leftrightarrows}} {}^{12}CH_3D \overset{^{12CH3D}k_{net}}{\rightarrow}. \quad (A3.2)$$

Following Section A2, we can write the steady state concentration of $^{12}CH_3D$ as

$$[^{12}CH_3D] = \frac{^{12+H}k_f[^{12}CH_2D\text{-S-CoM}][H] + {}^{12+D}k_f[^{12}CH_3\text{-S-CoM}][D]}{^{12-H}k_{rev} + {}^{12-D}k_{rev} + {}^{12CH3D}k_{net}}. \quad (A3.3)$$

Division of (A3.3) by (A2.4) yields:

$$\frac{[^{12}CH_3D]}{[^{12}CH_4]} = \left(\frac{^{12+H}k_f[^{12}CH_2D\text{-S-CoM}][H] + {}^{12+D}k_f[^{12}CH_3\text{-S-CoM}][D]}{^{12CH_3}k_f[^{12}CH_3\text{-S-CoM}][H]}\right) \times \left(\frac{^{12CH_4}k_{rev} + {}^{12CH_4}k_{net}}{^{12-H}k_{rev} + {}^{12-D}k_{rev} + {}^{12CH_3D}k_{net}}\right). \quad (A3.4)$$

We define the following ratios:

$$^{12CH_3D}R = \frac{[^{12}CH_3D]}{[^{12}CH_4]}; \quad ^{12CH_2D}R = \frac{[^{12}CH_2D\text{-S-CoM}]}{[^{12}CH_3\text{-S-CoM}]}; \quad \text{and} \quad ^{D}R = \frac{[D]}{[H]} \quad (A3.5a, b, \text{and } c)$$

Substituting (A3.5a, b and c) into (A3.4) and utilization of the algebra and simplifications introduced in Section A2 yields:

$$^{12CH_3D}R = \left(\frac{^{12+D}\kappa_f \times {}^{D}R + {}^{12+H}\kappa_f \times {}^{12CH_2D}R}{1 + r(^{12-D}\kappa_{rev} + {}^{12-H}\kappa_{rev} - 1)}\right). \quad (A3.6)$$

At metabolic equilibrium, the following isotope-exchange reaction is in isotopic equilibrium:

$$^{12}CH_3\text{-S-CoM} + D \leftrightarrows {}^{12}CH_2D\text{-S-CoM} + H. \quad (A3.7)$$

The equilibrium constant for this reaction is:

$$K_{eq}{}_{D \leftrightarrows ^{12}CH_2D\text{-S-CoM}} = \frac{^{12CH_2D}R}{^{D}R}. \quad (A3.8)$$

Substituting (A3.8) into (A3.6) gives

$$^{12CH_3D}R = {}^{D}R \times \left(\frac{^{12+D}\kappa_f + {}^{12+H}\kappa_f \times K_{eq}{}_{D \leftrightarrows ^{12}CH_2D\text{-S-CoM}}}{1 + r(^{12-D}\kappa_{rev} + {}^{12-H}\kappa_{rev} - 1)}\right) \quad (A3.9)$$

The fact that there are two pathways for making $^{12}CH_3D$ may have implications for understanding what controls the δD value of methane as well as its clumped isotopic composition. This is because these two paths could have very different isotope effects as one is a primary isotope effect, the addition of D, and the other is a secondary effect, the addition of H to an already deuterium-containing molecule. This could, perhaps, be recast as a mixing problem instead of a kinetic problem in which two distinct pools of $^{12}CH_3D$ (or $^{13}CH_3D$) are created at different rates and with different isotope effects. However, as there are few constraints on the sizes of these isotope effects (Scheller et al., 2013), we will simplify the problem by combing them into a single, amalgamated isotope effect:

$$^{12CH_3D}\kappa_f^* = {}^{12+D}\kappa_f + {}^{12+H}\kappa_f \times K_{eq}{}_{D \leftrightarrows ^{12}CH_2D\text{-S-CoM}} \quad (A3.10a)$$

and

$$^{12CH_3D}\kappa_{rev}^* = {}^{12-D}\kappa_{rev} + {}^{12-H}\kappa_{rev}. \quad (A3.10b)$$

This yields the following simplified equation:

$$^{12CH_3D}R = {}^{D}R \times \left(\frac{^{12CH_3D}\kappa_f^*}{1 + r(^{12CH_3D}\kappa_{rev}^* - 1)}\right). \quad (A3.11)$$

This greatly simplifies the equation, but it is critical to note that this form of the equation masks the true and interesting complexity of the reactions taking place. At equilibrium, r = 1, and

$$^{12CH_3D}R_{eq} = {}^{D}R_{eq} \times \frac{^{12CH_3D}\kappa_f^*}{^{12CH_3D}\kappa_{rev}^*}. \quad (A3.12)$$

Additionally at equilibrium, following Section A2, we can write the following isotope-exchange reaction:

$$^{12}CH_4 + D \leftrightarrows {}^{12}CH_3D + H. \quad (A3.13)$$

The equilibrium constant for this reaction is

$$\frac{^{12CH_3D}R_{eq}}{^{D}R_{eq}} = \frac{^{12CH_3D}\kappa_f^*}{^{12CH_3D}\kappa_{rev}^*} = K_{eq}{}_{D \leftrightarrows ^{12}CH_3D}. \quad (A3.14)$$

Problematically, ^{D}R is not measureable. We will presume, for simplicity, as discussed above, that the hydrogen and deuterium pool accessible to methane and methane precursors is in rapid equilibrium with the hydrogen and deuterium in water and that there is a constant offset between ^{D}R and $^{D}R_{H2O,liquid}$ (the D/H ratio of liquid H_2O). For simplicity, we will assume that they are equal. Any actual offset in this will be absorbed in $^{12CH_3D}\kappa_f^*$, and thus mathematically is unimportant. However, if the actual kinetic isotope effects of each individual step for methanogenesis are known, then using the exact value of the D/H ratio of the hydrogen donor to the methane precursor will be important. Regardless, for the derivation here, we assume,

$$^{D}R = \frac{[D]_{H2O}}{[H]_{H2O}} = {}^{H_2O}R. \quad (A3.15)$$

Inserting (A3.15) into (A3.14) yields:

$$\frac{^{12CH_3D}R_{eq}}{^{H_2O}R_{eq}} = \frac{^{12CH_3D}\kappa_f^*}{^{12CH_3D}\kappa_{rev}^*}. \quad (A3.16)$$

The ratio of $\frac{^{12CH_3D}R_{eq}}{^{H_2O}R_{eq}}$ is a calculable function of temperature (Richet et al., 1977; Horibe and Craig, 1995) and thus removes a degree of freedom from the model.

A.4. $^{13}CH_3D$ derivation

This section derives the $^{13}CH_3D/^{12}CH_4$ ratio as a function of the degree of reversibility of Eq. (A1.2). Following Sections A2 and A3, with similar symbology and assumptions, the following equation is found:

$$^{13}CH_3DR = \left(\frac{^{13+D}\kappa_f \times {}^{D}R \times {}^{13}CH_3R + {}^{13+H}\kappa_f \times {}^{13}CH_3DR}{1 + r(^{13-D}\kappa_{rev} + {}^{13-H}\kappa_{rev} - 1)}\right). \quad (A4.1)$$

where

$$^{13}CH_3DR = \frac{[^{13}CH_3D]}{[^{12}CH_4]} \text{ and } {}^{13}CH_2DR = \frac{[^{13}CH_2D\text{-S-CoM}]}{[^{12}CH_3\text{-S-CoM}]}. \quad (A4.2a \text{ and } b)$$

Using the constraints from metabolic equilibrium, the following isotope-exchange reaction can be written:

$$^{13}CH_3\text{-S-CoM} + D \leftrightarrows {}^{13}CH_2D\text{-S-CoM} + H \quad (A4.3)$$

such that:

$$\frac{\frac{^{13}CH_2D\text{-S-CoM}}{^{13}CH_3\text{-S-CoM}}}{{}^{D}R} = K_{eq}{}_{^{13}CH_3\text{-S-CoM} \leftrightarrows {}^{13}CH_2D\text{-S-CoM}}. \quad (A4.4)$$

Incorporating (A4.4) and (A2.13) into (A4.1) yields,

$$^{13}CH_3DR = {}^{D}R \times {}^{13}CO_2R \left(\frac{^{13+D}\kappa_f \times K_{eq}{}_{^{13}CO_2 \leftrightarrows {}^{13}CH_4} + {}^{13+H}\kappa_f \times K_{eq}{}_{^{13}CO_2 \leftrightarrows {}^{13}CH_4} \times K_{eq}{}_{^{13}CH_3\text{-S-CoM} \leftrightarrow {}^{13}CH_2D\text{-S-CoM}}}{1 + r(^{13-D}\kappa_{rev} + {}^{13-H}\kappa_{rev} - 1)}\right). \quad (A4.5)$$

As in Section 3, we define the following 'combined' fractionation factors:

$$^{13}CH_3D\kappa_f^* = {}^{13+D}\kappa_f \times K_{eq}{}_{^{13}CO_2 \leftrightarrows {}^{13}CH_4} + {}^{13+H}\kappa_f \times K_{eq}{}_{^{13}CO_2 \leftrightarrows {}^{13}CH_4} \times K_{eq}{}_{^{13}CH_3\text{-S-CoM} \leftrightarrows {}^{13}CH_2D\text{-S-CoM}} \quad (A4.6a)$$

and

$$^{13}CH_3D\kappa_{rev}^* = {}^{13-D}\kappa_{rev} + {}^{13-H}\kappa_{rev} \quad (A4.6b)$$

Substituting (A4.6) into (A4.5) gives

$$^{13}CH_3DR = {}^{D}R \times {}^{13}CO_2R \left(\frac{^{13}CH_3D\kappa_f^*}{1 + r(^{13}CH_3D\kappa_{rev}^* - 1)}\right). \quad (A4.7)$$

At $r = 1$, the following homogenous-phase equilibrium reaction occurs:

$$^{12}CH_3D + {}^{13}CH_4 \leftrightarrows {}^{12}CH_4 + {}^{13}CH_3D. \quad (A4.8)$$

The equilibrium constant for (A4.8) is

$$K_{eq}{}_{^{13}CH_3D} = \frac{[^{12}CH_4]_{eq}[^{13}CH_3D]_{eq}}{[^{12}CH_3D]_{eq}[^{13}CH_4]_{eq}}, \quad (A4.9)$$

which is a known function of temperature (Bottinga, 1969; Ma et al., 2008; Cao and Liu, 2012; Stolper et al., 2014a; Ono et al., 2014a; Webb and Miller, 2014). Following some algebraic manipulations, we can write:

$$K_{eq}{}_{^{13}CH_3D} \times \left(\frac{^{13}CH_3\kappa_f^*}{^{13}CH_4\kappa_{rev}}\right) \times \left(\frac{^{12}CH_3D\kappa_f^*}{^{12}CH_3D\kappa_{rev}^*}\right) = \frac{^{13}CH_3D\kappa_f^*}{^{13}CH_3D\kappa_{rev}^*}, \quad (A4.10)$$

which removes a degree of freedom from the model.

A.5. $^{12}CH_2D_2$ derivation

This section derives the $^{12}CH_2D_2/^{12}CH_4$ ratio as a function of the degree of reversibility of Eq. (A1.2). Following Sections A2–A4, with similar symbology and assumptions, the following equation is found:

$$^{12}CH_2D_2R = \left(\frac{^{H_2D+D}\kappa_f \times {}^{D}R \times {}^{12}CH_2DR + {}^{HD_2+H}\kappa_f \times {}^{12}CHD_2R}{1 + r(^{H_2D_2-D}\kappa_{rev} + {}^{H_2D_2-H}\kappa_{rev} - 1)}\right) \quad (A5.1)$$

where,

$$^{12}CHD_2R = \frac{[^{12}CHD_2\text{-S-CoM}]}{[^{12}CH_3\text{-S-CoM}]}. \quad (A5.2)$$

Using constraints from metabolic equilibrium, we write

$$^{12}CH_2D\text{-S-CoM} + D \leftrightarrows {}^{12}CHD_2\text{-S-CoM} + H \quad (A5.3)$$

with the following equilibrium constant:

$$\frac{\frac{^{12}CHD_2\text{-S-CoM}}{^{12}CH_2D\text{-S-CoM}}}{{}^{D}R} = K_{eq}{}_{^{12}CH_2D\text{-S-CoM} \leftrightarrows {}^{12}CHD_2\text{-S-CoM}}. \quad (A5.4)$$

Combination of (A5.4) with (A3.8) yields

$$^{12}CHD_2R = ({}^{D}R)^2 \times K_{eq}{}_{^{12}CH_2D\text{-S-CoM} \leftrightarrows {}^{12}CHD_2\text{-S-CoM}} \times K_{eq}{}_{D \leftrightarrows {}^{12}CH_2D\text{-S-CoM}}. \quad (A5.5)$$

Combining (A5.5) and (A3.8) with (A5.1) yields

$$^{12}CH_2D_2R = ({}^{D}R)^2 \times \left(\frac{^{H_2D+D}\kappa_f \times K_{eq}{}_{D \leftrightarrows {}^{12}CH_2D\text{-S-CoM}} + {}^{HD_2+H}\kappa_f \times K_{eq}{}_{^{12}CH_2D\text{-S-CoM} \leftrightarrows {}^{12}CHD_2\text{-S-CoM}} \times K_{eq}{}_{D \leftrightarrows {}^{12}CH_2D\text{-S-CoM}}}{1 + r(^{H_2D_2-D}\kappa_{rev} + {}^{H_2D_2-H}\kappa_{rev} - 1)}\right). \quad (A5.6)$$

Rewriting with the following 'combined' fractionation factors:

$$
\begin{aligned}
{}^{12}CH_2D_2\kappa_f^* = {}& {}^{H_2D+D}\kappa_f \times \frac{K_{eq}}{D\leftrightarrows{}^{12}CH_2D\text{-S-CoM}} \\
& + {}^{HD_2+H}\kappa_f \\
& \times \frac{K_{eq}}{{}^{12}CH_2D\text{-S-CoM}\leftrightarrows{}^{12}CHD_2\text{-S-CoM}} \\
& \times \frac{K_{eq}}{D\leftrightarrows{}^{12}CH_2D\text{-S-CoM}}
\end{aligned}
\tag{5.7a}
$$

and

$$
{}^{12}CH_2D_2\kappa_{rev}^* = {}^{H_2D_2\text{-}D}\kappa_{rev} + {}^{H_2D_2-H}\kappa_{rev}, \tag{A5.7b}
$$

this equation becomes

$$
{}^{12}CH_2D_2R = ({}^{D}R)^2 \times \left(\frac{{}^{12}CH_2D_2\kappa_f^*}{1 + r({}^{12}CH_2D_2\kappa_{rev}^* - 1)}\right). \tag{A5.8}
$$

At $r = 1$, the following equilibrium reaction occurs:

$$
{}^{12}CH_3D + {}^{12}CH_3D \leftrightarrows {}^{12}CH_4 + {}^{12}CH_2D_2, \tag{A5.9}
$$

with the equilibrium constant

$$
K_{eq}_{{}^{12}CH_2D_2} = \frac{[{}^{12}CH_4]_{eq}[{}^{12}CH_2D_2]_{eq}}{[{}^{12}CH_3D]^2_{eq}}, \tag{A5.10}
$$

which, as discussed in Section A4, is a function of temperature and thus removes a degree of freedom from the model.

With some algebraic manipulation, this can be rewritten for convenience as

$$
K_{eq}_{{}^{12}CH_2D_2} \times \left(\frac{{}^{12}CH_3D\kappa_f^*}{{}^{12}CH_3D\kappa_{rev}^*}\right)^2 = \frac{{}^{12}CH_2D_2\kappa_f^*}{{}^{12}CH_2D_2\kappa_{rev}^*}. \tag{A5.11}
$$

REFERENCES

Apotria T. and Kaiser C. (1994). In *Fracturing and Stress History of the Devonian Antrim Shale, Michigan Basin* (eds. P. Nelson and S. Lauback). Rock Mechanics, pp. 809–816.

Balabane M., Galimov E., Hermann M. and Letolle R. (1987) Hydrogen and carbon isotope fractionation during experimental production of bacterial methane. *Org. Geochem.* **11**, 115–119.

Bernard B. B., Brooks J. M. and Sackett W. M. (1976) Natural gas seepage in the Gulf of Mexico. *Earth Planet. Sci. Lett.* **31**, 48–54.

Bigeleisen J. and Wolfsberg M. (1958) Theoretical and experimental aspects of isotope effects in chemical kinetics. *Adv. Chem. Phys.*, 15–76.

Bilek R., Tyler S., Kurihara M. and Yagi K. (2001) Investigation of cattle methane production and emission over a 24-hour period using measurements of $\delta^{13}C$ and δD of emitted CH_4 and rumen water. *J. Geophys. Res. Atmos. (1984–2012)* **106**, 15405–15413.

Blair N. (1998) The $\delta^{13}C$ of biogenic methane in marine sediments: the influence of C_{org} deposition rate. *Chem. Geol.* **152**, 139–150.

Boone D. R., Johnson R. L. and Liu Y. (1989) Diffusion of the interspecies electron carriers H_2 and formate in methanogenic ecosystems and its implications in the measurement of K_m for H_2 or formate uptake. *Appl. Environ. Microbiol.* **55**, 1735–1741.

Bottinga Y. (1969) Calculated fractionation factors for carbon and hydrogen isotope exchange in the system calcite–carbon dioxide–graphite–methane–hydrogen–water vapor. *Geochim. Cosmochim. Acta* **33**, 49–64.

Botz R., Pokojski H.-D., Schmitt M. and Thomm M. (1996) Carbon isotope fractionation during bacterial methanogenesis by CO_2 reduction. *Org. Geochem.* **25**, 255–262.

Bradley A., Leavitt W. and Johnston D. (2011) Revisiting the dissimilatory sulfate reduction pathway. *Geobiology* **9**, 446–457.

Brunner B. and Bernasconi S. M. (2005) A revised isotope fractionation model for dissimilatory sulfate reduction in sulfate reducing bacteria. *Geochim. Cosmochim. Acta* **69**, 4759–4771.

Brunner B., Bernasconi S. M., Kleikemper J. and Schroth M. H. (2005) A model for oxygen and sulfur isotope fractionation in sulfate during bacterial sulfate reduction processes. *Geochim. Cosmochim. Acta* **69**, 4773–4785.

Burke, Jr, R. A. (1993) Possible influence of hydrogen concentration on microbial methane stable hydrogen isotopic composition. *Chemosphere* **26**, 55–67.

Cao X. and Liu Y. (2012) Theoretical estimation of the equilibrium distribution of clumped isotopes in nature. *Geochim. Cosmochim. Acta* **77**, 292–303.

Cercone K. and Pollack H. (1991) Thermal maturity of the Michigan Basin. *Geol. Soc. Am. Spec. Papers* **256**, 1–12.

Chung H., Gormly J. and Squires R. (1988) Origin of gaseous hydrocarbons in subsurface environments: theoretical considerations of carbon isotope distribution. *Chem. Geol.* **71**, 97–104.

Claypool G. E. and Kaplan I. (1974) The origin and distribution of methane in marine sediments. *Natural Gases in Marine Sediments*. Springer, pp. 99–139.

Clog, M., Martini, A., Lawson, M., Eiler, J., 2014. Doubly ^{13}C-substituted ethane in shale gases, Goldschmidt Conference. *Mineralogical Conference, Sacremento, CA*, p. 435.

Conrad R. (2005) Quantification of methanogenic pathways using stable carbon isotopic signatures: a review and a proposal. *Org. Geochem.* **36**, 739–752.

Criss R. E. (1999) *Principles of Stable Isotope Distribution*. Oxford University Press, New York.

Curtis J. B. (2002) Fractured shale-gas systems. *AAPG Bull.* **86**, 1921–1938.

Daniels L., Fulton G., Spencer R. and Orme-Johnson W. (1980) Origin of hydrogen in methane produced by *Methanobacterium thermoautotrophicum*. *J. Bacteriol.* **141**, 694–698.

Duffy M., Kinnaman F. S., Valentine D. L., Keller E. A. and Clark J. F. (2007) Gaseous emission rates from natural petroleum seeps in the Upper Ojai Valley, California. *Environ. Geosci.* **14**, 197–207.

Edwards K. J., Becker K. and Colwell F. (2012) The deep, dark energy biosphere: intraterrestrial life on Earth. *Annu. Rev. Earth Planet. Sci.* **40**, 551–568.

Eiler J. M. (2007) "Clumped-isotope" geochemistry – the study of naturally-occurring, multiply-substituted isotopologues. *Earth Planet. Sci. Lett.* **262**, 309–327.

Eiler J. M. (2013) The isotopic anatomies of molecules and minerals. *Annu. Rev. Earth Planet. Sci.* **41**, 411–441.

Eiler J. M., Bergquist B., Bourg I., Cartigny P., Farquhar J., Gagnon A., Guo W., Halevy I., Hofmann A., Larson T. E., Levin N., Schauble E. A. and Stolper D. (2014a) Frontiers of stable isotope geoscience. *Chem. Geol.* **372**, 119–143.

Eiler, J. M., Clog, M., Kitchen, N., Stolper, D. (2014b) Mass spectrometric analysis of $^{12}CH_2D_2$, *2014 Clumped-Isotope Workshop*, Zurich, Switzerland.

Eiler J. M., Clog M., Magyar P., Piasecki A., Sessions A., Stolper D., Deerberg M., Schlueter H.-J. and Schwieters J. (2013) A high-resolution gas-source isotope ratio mass spectrometer. *Int. J. Mass Spectrom.* **335**, 45–56.

Eiler J. M. and Schauble E. (2004) $^{18}O^{13}C^{16}O$ in Earth's atmosphere. *Geochim. Cosmochim. Acta* **68**, 4767–4777.

England W., Mackenzie A., Mann D. and Quigley T. (1987) The movement and entrapment of petroleum fluids in the subsurface. *J. Geol. Soc.* **144**, 327–347.

Farquhar J., Johnston D. T., Wing B. A., Habicht K. S., Canfield D. E., Airieau S. and Thiemens M. H. (2003) Multiple sulphur isotopic interpretations of biosynthetic pathways: implications for biological signatures in the sulphur isotope record. *Geobiology* **1**, 27–36.

Feakins S. J. and Sessions A. L. (2010) Controls on the D/H ratios of plant leaf waxes in an arid ecosystem. *Geochim. Cosmochim. Acta* **74**, 2128–2141.

Formolo M., Salacup J., Petsch S., Martini A. and Nüsslein K. (2008) A new model linking atmospheric methane sources to Pleistocene glaciation via methanogenesis in sedimentary basins. *Geology* **36**, 139–142.

Fuchs G., Thauer R., Ziegler H. and Stichler W. (1979) Carbon isotope fractionation by *Methanobacterium thermoautotrophicum*. *Arch. Microbiol.* **120**, 135–139.

Gruen, D. S., Wang, D. T., Stewart, L., Holden, J., Ono, S. (2014) Clumped isotope systematics of biogenic methane. *Goldschmidt Conference*. Mineralogical Magazine, Sacramento, CA, p. 868.

Gutschick R. C. and Sandberg C. A. (1991) Late Devonian history of Michigan basin. *Geol. Soc. Am. Spec. Papers* **256**, 181–202.

Hallam S. J., Putnam N., Preston C. M., Detter J. C., Rokhsar D., Richardson P. M. and DeLong E. F. (2004) Reverse methanogenesis: testing the hypothesis with environmental genomics. *Science* **305**, 1457–1462.

Hattori S., Nashimoto H., Kimura H., Koba K., Yamada K., Shimizu M., Watanabe H., Yoh M. and Yoshida N. (2012) Hydrogen and carbon isotope fractionation by thermophilic hydrogenotrophic methanogens from a deep aquifer under coculture with fermenters. *Geochem. J.* **46**, 193–200.

Hayes J. M. (2001) Fractionation of carbon and hydrogen isotopes in biosynthetic processes. *Rev. Mineral. Geochem.* **43**, 225–277.

Horibe Y. and Craig H. (1995) D/H fractionation in the system methane–hydrogen–water. *Geochim. Cosmochim. Acta* **59**, 5209–5217.

Horita J. and Wesolowski D. J. (1994) Liquid–vapor fractionation of oxygen and hydrogen isotopes of water from the freezing to the critical temperature. *Geochim. Cosmochim. Acta* **58**, 3425–3437.

Hunt J. M. (1996) *Petroleum Geochemistry and Geology*. W. H. Freeman and Company, New York.

Kawagucci S., Kobayashi M., Hattori S., Yamada K., Ueno Y., Takai K. and Yoshida N. (2014) Hydrogen isotope systematics among H_2–H_2O–CH_4 during the growth of the hydrogenotrophic methanogen Methanothermobacter thermoautotrophicus strain ΔH. *Geochim. Cosmochim. Acta*.

Kinnaman F. S., Valentine D. L. and Tyler S. C. (2007) Carbon and hydrogen isotope fractionation associated with the aerobic microbial oxidation of methane, ethane, propane and butane. *Geochim. Cosmochim. Acta* **71**, 271–283.

Kirk M. F., Martini A. M., Breecker D. O., Colman D. R., Takacs-Vesbach C. and Petsch S. T. (2012) Impact of commercial natural gas production on geochemistry and microbiology in a shale-gas reservoir. *Chem. Geol.* **332**, 15–25.

Kniemeyer O., Musat F., Sievert S. M., Knittel K., Wilkes H., Blumenberg M., Michaelis W., Classen A., Bolm C. and Joye S. B. (2007) Anaerobic oxidation of short-chain hydrocarbons by marine sulphate-reducing bacteria. *Nature* **449**, 898–901.

Kreuzer-Martin H. W., Ehleringer J. R. and Hegg E. L. (2005) Oxygen isotopes indicate most intracellular water in log-phase *Escherichia coli* is derived from metabolism. *Proc. Natl. Acad. Sci. U.S.A.* **102**, 17337–17341.

Luczaj J. A., Harrison, III, W. B. and Williams N. S. (2006) Fractured hydrothermal dolomite reservoirs in the Devonian Dundee Formation of the central Michigan Basin. *AAPG Bull.* **90**, 1787–1801.

Ma L., Castro M. C., Hall C. M. and Walter L. M. (2005) *Cross-formational flow and salinity sources inferred from a combined study of helium concentrations, isotopic ratios, and major elements in the Marshall aquifer, southern Michigan*. Geochem. Geophys. Geosyst., 6.

Ma Q., Wu S. and Tang Y. (2008) Formation and abundance of doubly-substituted methane isotopologues ($^{13}CH_3D$) in natural gas systems. *Geochim. Cosmochim. Acta* **72**, 5446–5456.

Martini A., Walter L., Budai J., Ku T., Kaiser C. and Schoell M. (1998) Genetic and temporal relations between formation waters and biogenic methane: Upper Devonian Antrim Shale, Michigan Basin, USA. *Geochim. Cosmochim. Acta* **62**, 1699–1720.

Martini A. M., Budai J. M., Walter L. M. and Schoell M. (1996) Microbial generation of economic accumulations of methane within a shallow organic-rich shale. *Nature* **383**, 155–158.

Martini A. M., Walter L. M., Ku T. C., Budai J. M., McIntosh J. C. and Schoell M. (2003) Microbial production and modification of gases in sedimentary basins: a geochemical case study from a Devonian shale gas play, Michigan basin. *AAPG Bull.* **87**, 1355–1375.

Martini A. M., Walter L. M. and McIntosh J. C. (2008) Identification of microbial and thermogenic gas components from Upper Devonian black shale cores, Illinois and Michigan basins. *AAPG Bull.* **92**, 327–339.

McIntosh J., Garven G. and Hanor J. (2011) Impacts of Pleistocene glaciation on large-scale groundwater flow and salinity in the Michigan Basin. *Geofluids* **11**, 18–33.

McIntosh J. and Walter L. (2005) Volumetrically significant recharge of pleistocene glacial meltwaters into epicratonic basins: constraints imposed by solute mass balances. *Chem. Geol.* **222**, 292–309.

Ni Y., Ma Q., Ellis G. S., Dai J., Katz B., Zhang S. and Tang Y. (2011) Fundamental studies on kinetic isotope effect (KIE) of hydrogen isotope fractionation in natural gas systems. *Geochim. Cosmochim. Acta* **75**, 2696–2707.

Ono S., Wang D. T., Gruen D. S., Sherwood Lollar B., Zahniser M. S., McManus B. J. and Nelson D. D. (2014a) Measurement of a doubly substituted methane isotopologue, $^{13}CH_3D$, by tunable infrared laser direct absorption spectroscopy. *Anal. Chem.* **86**, 6487–6494.

Ono, S., Wang, D., Gruen, D., Sherwood Lollar, B., Mcmanus, B., Zahniser, M., Nelson, D. (2014) Measurements of clumped methane isotopologue ($^{13}CH_3D$) by tunable mid-infrared laser spectroscopy. *Goldschmidt Conference*. Mineralogical Magazine, Sacramento, CA, p. 1870.

Osborn S. G. and McIntosh J. C. (2010) Chemical and isotopic tracers of the contribution of microbial gas in Devonian organic-rich shales and reservoir sandstones, northern Appalachian Basin. *Appl. Geochem.* **25**, 456–471.

Penning H., Plugge C. M., Galand P. E. and Conrad R. (2005) Variation of carbon isotope fractionation in hydrogenotrophic methanogenic microbial cultures and environmental samples at different energy status. *Glob. Change Biol.* **11**, 2103–2113.

Price L. C. and Schoell M. (1995) Constraints on the origins of hydrocarbon gas from compositions of gases at their site of origin. *Nature* **378**, 368–371.

Quigley T. and Mackenzie A. (1988) The temperatures of oil and gas formation in the sub-surface. *Nature* **333**, 549–552.

Rees C. (1973) A steady-state model for sulphur isotope fractionation in bacterial reduction processes. *Geochim. Cosmochim. Acta* **37**, 1141–1162.

Richet P., Bottinga Y. and Janoy M. (1977) A review of hydrogen, carbon, nitrogen, oxygen, sulphur, and chlorine stable isotope

enrichment among gaseous molecules. *Annu. Rev. Earth Planet. Sci.* **5**, 65–110.

Schauble E. A., Ghosh P. and Eiler J. M. (2006) Preferential formation of ^{13}C–^{18}O bonds in carbonate minerals, estimated using first-principles lattice dynamics. *Geochim. Cosmochim. Acta* **70**, 2510–2529.

Scheller S., Goenrich M., Boecher R., Thauer R. K. and Jaun B. (2010) The key nickel enzyme of methanogenesis catalyses the anaerobic oxidation of methane. *Nature* **465**, 606–608.

Scheller S., Goenrich M., Thauer R. K. and Jaun B. M. (2013) Methyl-coenzyme M reductase from methanogenic archaea: isotope effects on the formation and anaerobic oxidation of methane. *J. Am. Chem. Soc.* **135**(40), 14985–14995. http://dx.doi.org/10.1021/ja4064876.

Schimmelmann A., Sessions A. L. and Mastalerz M. (2006) Hydrogen isotopic (D/H) composition of organic matter during diagenesis and thermal maturation. *Annu. Rev. Earth Planet. Sci.* **34**, 501–533.

Schlegel M. E., Zhou Z., McIntosh J. C., Ballentine C. J. and Person M. A. (2011) Constraining the timing of microbial methane generation in an organic-rich shale using noble gases, Illinois Basin, USA. *Chem. Geol.* **287**, 27–40.

Schoell M. (1980) The hydrogen and carbon isotopic composition of methane from natural gases of various origins. *Geochim. Cosmochim. Acta* **44**, 649–661.

Schoell M. (1983) Genetic characterization of natural gases. *AAPG Bull.* **67**, 2225–2238.

Seewald J. S. (2003) Organic–inorganic interactions in petroleum-producing sedimentary basins. *Nature* **426**, 327–333.

Seewald J. S., Benitez-Nelson B. C. and Whelan J. K. (1998) Laboratory and theoretical constraints on the generation and composition of natural gas. *Geochim. Cosmochim. Acta* **62**, 1599–1617.

Stolper D. A., Sessions A. L., Ferreira A., Santos Neto E. V., Schimmelmann A., Shusta S. S., Valentine D. L. and Eiler J. M. (2014a) Combined ^{13}C–D and D–D clumping in methane: methods and preliminary results. *Geochim. Cosmochim. Acta* **126**, 169–191.

Stolper D., Lawson M., Davis C., Ferreira A., Neto E. S., Ellis G., Lewan M., Martini A., Tang Y. and Schoell M. (2014b) Formation temperatures of thermogenic and biogenic methane. *Science* **344**, 1500–1503.

Stolper D. A., Davis C. L., Eiler J. M., Ellis G. S., Ferreira A. A., Lawson M., Martini A. M., Santos Neto E. V., Schoell M., Sessions A. L., Shusta S. S., Tang Y. and Valentine D. L. (2014c) *Clumped Isotopes of Methane: Applications to Both Low and High Temperature Natural Systems*. Mineralogical Magazine, Sacremento, CA, p. 2393.

Sugimoto A. and Wada E. (1995) Hydrogen isotopic composition of bacterial methane: CO_2/H_2 reduction and acetate fermentation. *Geochim. Cosmochim. Acta* **59**, 1329–1337.

Takai K., Nakamura K., Toki T., Tsunogai U., Miyazaki M., Miyazaki J., Hirayama H., Nakagawa S., Nunoura T. and Horikoshi K. (2008) Cell proliferation at 122 °C and isotopically heavy CH_4 production by a hyperthermophilic methanogen under high-pressure cultivation. *Proc. Natl. Acad. Sci.* **105**, 10949–10954.

Tang Y., Perry J., Jenden P. and Schoell M. (2000) Mathematical modeling of stable carbon isotope ratios in natural gases. *Geochim. Cosmochim. Acta* **64**, 2673–2687.

Thauer R. K. (1998) Biochemistry of methanogenesis: a tribute to Marjory Stephenson. *Microbiology* **144**, 2377–2406.

Thauer R. K. (2011) Anaerobic oxidation of methane with sulfate: on the reversibility of the reactions that are catalyzed by enzymes also involved in methanogenesis from CO_2. *Curr. Opin. Microbiol.* **14**, 292–299.

Thauer R. K., Kaster A.-K., Seedorf H., Buckel W. and Hedderich R. (2008) Methanogenic archaea: ecologically relevant differences in energy conservation. *Nat. Rev. Microbiol.* **6**, 579–591.

Tissot B. P. and Welte D. H. (1978) *Petroleum Formation and Occurrence: A New Approach to Oil and Gas Exploration*. Springer-Verlag, Berlin.

Tsuji K., Teshima H., Sasada H. and Yoshida N. (2012) Spectroscopic isotope ratio measurement of doubly-substituted methane. *Spectrochim. Acta A Mol. Biomol. Spectrosc.* **98**, 43–46.

Urey H. C. and Rittenberg D. (1933) Some thermodynamic properties of the H^1H^1, H^2H^2 molecules and compounds containing the H^2 atom. *J. Chem. Phys.* **1**, 137.

Valentine D. L. (2011) Emerging topics in marine methane biogeochemistry. *Annu. Rev. Mar. Sci.* **3**, 147–171.

Valentine D. L., Chidthaisong A., Rice A., Reeburgh W. S. and Tyler S. C. (2004) Carbon and hydrogen isotope fractionation by moderately thermophilic methanogens. *Geochim. Cosmochim. Acta* **68**, 1571–1590.

Valentine D. L., Kessler J. D., Redmond M. C., Mendes S. D., Heintz M. B., Farwell C., Hu L., Kinnaman F. S., Yvon-Lewis S. and Du M. (2010) Propane respiration jump-starts microbial response to a deep oil spill. *Science* **330**, 208–211.

Waldron P. J., Petsch S. T., Martini A. M. and Nüsslein K. (2007) Salinity constraints on subsurface archaeal diversity and methanogenesis in sedimentary rock rich in organic matter. *Appl. Environ. Microbiol.* **73**, 4171–4179.

Wang, D.T., Gruen, D.S., Sherwood Lollar, B., Hinrichs, K.-U., Stewart, L.C., Holden, J.F., Hristov, A.N., Pohlman, J.W., Morrill, P.L., Konneke, M., Delwiche, K.B., Reeves, E.P., Sutcliffe, C.N., Ritter, D.J., Seewald, J.S., McIntosh, J.C., Hemond, H.F., Kubo, M.D., Cardace, D., Hoehler, T.M., Ono, S. (in press). Nonequilibrium clumped isotope signals in microbial methane. *Science*.

Wang Z., Schauble E. A. and Eiler J. M. (2004) Equilibrium thermodynamics of multiply substituted isotopologues of molecular gases. *Geochim. Cosmochim. Acta* **68**, 4779–4797.

Webb M. A. and Miller, III, T. F. (2014) Position-specific and clumped stable isotope studies: comparison of the Urey and path-integral approaches for carbon dioxide, nitrous oxide, methane, and propane. *J. Phys. Chem A* **118**, 467–474.

Whiticar M. J. (1999) Carbon and hydrogen isotope systematics of bacterial formation and oxidation of methane. *Chem. Geol.* **161**, 291–314.

Whiticar M. J., Faber E. and Schoell M. (1986) Biogenic methane formation in marine and freshwater environments: CO_2 reduction vs acetate fermentation—isotope evidence. *Geochim. Cosmochim. Acta* **50**, 693–709.

Wilhelms A., Larter S., Head I., Farrimond P., Di-Primio R. and Zwach C. (2001) Biodegradation of oil in uplifted basins prevented by deep-burial sterilization. *Nature* **411**, 1034–1037.

Wilson T. P. and Long D. T. (1993) Geochemistry and isotope chemistry of Michigan Basin brines: Devonian formations. *Appl. Geochem.* **8**, 81–100.

Wing B. A. and Halevy I. (2014) Intracellular metabolite levels shape sulfur isotope fractionation during microbial sulfate respiration. *Proc. Natl. Acad. Sci.*, 201407502.

Wuchter C., Banning E., Mincer T. J., Drenzek N. J. and Coolen M. J. (2013) Microbial diversity and methanogenic activity of Antrim Shale formation waters from recently fractured wells. *Front. Microbiol.* **4**.

Wuebbles D. J. and Hayhoe K. (2002) Atmospheric methane and global change. *Earth Sci. Rev.* **57**, 177–210.

Yeung L. Y., Young E. D. and Schauble E. A. (2012) Measurements of $^{18}O^{18}O$ and $^{17}O^{18}O$ in the atmosphere and

the role of isotope-exchange reactions. *J. Geophys. Res.* **117**. http://dx.doi.org/10.1029/2012JD017992.

Yoshinaga M. Y., Holler T., Goldhammer T., Wegener G., Pohlman J. W., Brunner B., Kuypers M. M., Hinrichs K.-U. and Elvert M. (2014) Carbon isotope equilibration during sulphate-limited anaerobic oxidation of methane. *Nat. Geosci.*

Yoshioka H., Sakata S. and Kamagata Y. (2008) Hydrogen isotope fractionation by *Methanothermobacter thermoautotrophicus* in coculture and pure culture conditions. *Geochim. Cosmochim. Acta* **72**, 2687–2694.

Zhang Y. (1994) Reaction kinetics, geospeedometry, and relaxation theory. *Earth Planet. Sci. Lett.* **122**, 373–391.

Associate editor: Ed Hornibrook